EFFICIENCY IMPROVEMENTS OF AN AXIAL FLUX PERMANENT MAGNET MOTOR

A Thesis

by

YICHI ZHANG

Submitted to the Office of Graduate and Professional Studies of
Texas A&M University
in partial fulfillment of the requirements for the degree of

MASTER OF SCIENCE

Chair of Committee, Hamid Toliyat
Committee Members, Shanker Bhattacharyya
Katherine Davis
Won-jong Kim
Head of Department, Miroslav Begovic

August 2019

Major Subject: Electrical Engineering

ABSTRACT

NovaMax® motor is an axial flux permanent magnet (PM) motor which incorporates several unique topologies to achieve state-of-the-art efficiency of 96%. The use of grain oriented electric steel (GOES) increases permeability along the axial flux path; the use of soft magnet composite (SMC) allows rotor flux to be concentrated from all directions; and the use of conical air gap increases the surface area of the air gap and, thus, increases total magnetic flux. While the NovaMax is one of the most efficient permanent magnet motors on the market, the goal of this research project is to optimize the current NovaMax's design to further reduce the motor loss by 20%.

This project consists of two phases. First phase is to develop a parametric 3D finite element analysis (FEA) model of the current motor. In order for the model to accurately predict the motor behavior, a set of experimental testing of the current NovaMax motor is conducted for results comparison between the simulation and testing. Additionally, an air gap study motor, in which the air gap can be changed, is tested to further correlate the ANSYS model to the actual motor.

Second phase is the motor efficiency improvements using FEA model developed. A set of new design changes including new motor geometry and change in magnetic material have been proposed and tested in the FEA model. After adoption of some proposed ideas, the motor loss is reduced by 20.9% compared to the current motor.

While working on this research project, the cost and manufacturability are also considered to allow this motor be commercialized for energy saving across the country.

DEDICATION

To my family

ACKNOWLEDGEMENTS

I would like to thank my committee chair, Dr. Toliyat, and my committee members, Dr. Bhattacharyya, Dr. Davis, Dr. Kim, for their guidance and support throughout the course of this research.

Thanks to my friends and colleagues Matthew Gardner, Dorsa Talebi and Matthew Johnson for their time and collaboration while working on this research project.

Thanks also to Paul Kanuer, Alan Crapo and Harold Willis from Regal Beloit for their collaboration and feedback on this project.

I would like to thank Texas A&M High Performance Research Computing as portions of this research were conducted with the advanced computing resources provided by them.

Finally, thanks to my parents for their support and encouragement.

CONTRIBUTORS AND FUNDING SOURCES

Contributors

This work was supervised by Dr. Hamid A. Toliyat [advisor], Dr. Shankar P. Bhattacharyya and Dr. Katherine Davis of the Department of Electrical and Computer Engineering, and Professor Won-Jong Kim of the Department of Mechanical Engineering.

Part of the testing data and ideas for design changes of NovaMax motor were provided by Paul Knauer, Alan Crapo and Harold Willis from Regal Beloit. Matlab scripts for creating figures and plots are developed based on scripts provided by Matthew Gardner and Matthew Johnson from Advanced Electric Machines and Power Electronics (EMPE) lab. Parametric model for current motor is developed with help from Matthew Gardner and Dorsa Talebi from EMPE lab.

All other work conducted for the thesis was completed by the student independently.

Funding Sources

Graduate study was supported by a fellowship from Texas A&M University.

Regal Beloit has provided hardware including NovaMax motor, torque meter and motor drives etc.

This work was also made possible in part by the US Department of Energy under Grant Number DE/EE-0007875. Its contents are solely the responsibility of the authors and do not necessarily represent the official views of the US Department of Energy.

NOMENCLATURE

DOE	US Department of Energy
Back-EMF	Counter-Electromotive Force
FEA	Finite Element Analysis
GOES	Grain Oriented Electrical Steel
ID	Interior Diameter
MUT	Motor under Test
OD	Outer Diameter
PM	Permanent Magnet
PP	Pole Pairs
RMS	Root Mean Square
RPM	Revolutions per Minute
SMC	Soft Magnet Composite
VFD	Variable Frequency Drive

TABLE OF CONTENTS

Page

ABSTRACT ii

DEDICATION iv

ACKNOWLEDGEMENTS v

CONTRIBUTORS AND FUNDING SOURCES vi

NOMENCLATURE vii

TABLE OF CONTENTS viii

LIST OF FIGURES x

LIST OF TABLES xiii

1. INTRODUCTION 1

1.1. Overview of NovaMax Motor 2
1.2. Steps to Optimize the Motor Design 4
1.3. Future Steps 6

2. DEVELOPING AN ACCURATE 3D PARAMETRIC MODEL 8

2.1. Initial Model Development 8
2.2. Motor Loss Breakdown and FEA model Correlation 11
2.2.1. Mechanical Losses 11
2.2.2. Copper Loss 15
2.2.3. Electromagnetic Losses 17
2.2.4. Air Gap Study 19
2.2.5. Correlating the Model to the Experimental Data 27
2.3. Loss Breakdown Comparison 32

3. IMPACT OF SWITCHING FREQUENCY ON MOTOR LOSSES AND TORQUE 35

3.1. Theoretical Analysis of Impact of Switching Frequencies on Losses 35
3.2. Theoretical Analysis of Impact of Switching Frequencies on Torque 40
3.3. FEA of Motor Losses and Torque Ripple 44

3.4. Conclusion on Impact of Switching Frequency on Motor Performance 47

4. DESIGN CHANGES FOR EFFICIENCY IMPROVEMENTS 49

4.1. Reduced Volume of Stator Teeth 49
4.1.1. Stator Teeth Length Reduction 50
4.1.2. Stator Teeth Cross Section Area Reduction 52
4.2. Stator Caps 54
4.2.1. Optimizing the Cap Shape and Size 55
4.2.2. Bridged Shaped Stator Caps 57
4.3. Increasing the Effective Air Gap Area 58
4.3.1. Flatten the Stator OD 59
4.3.2. Sharper SMC Pole Edge 61
4.4. Optimal Air Gap Length Evaluation 63
4.5. Other Attempted Design Changes 66
4.5.1. Slits in Stator Teeth 66
4.5.2. NdFeB Magnets to Replace the Existing Ferrite Magnets 68

5. CONCLUSIONS AND FUTURE STEPS 72

5.1. Conclusions 72
5.2. Future Steps 73

REFERENCES 75

LIST OF FIGURES

Page

Figure 1.1 Transverse-section view of NovaMax motor with red arrows illustrating flux direction....1

Figure 1.2 Cross-section view of one rotor of NovaMax motor with red arrows illustrating flux direction 3

Figure 1.3 View of NovaMax motor with one rotor removed 4

Figure 1.4 Experimental test setup with protective enclosure removed 5

Figure 2.1 NovaMax FEA model of (a) rotor with casing, (b) stator teeth with winding, (c) full motor.....9

Figure 2.2 NovaMax FEA rotor model of (a) normal motor (b) different magnet thicknesses (c) more pole pairs.....10

Figure 2.3 Room temperature no-load losses in the normal motor....13

Figure 2.4 Room temperature no-load losses in the non-magnetized motor 13

Figure 2.5 Variation of no load loss with end plate temperature and speed for the motor with no fan or seals. 14

Figure 2.6 Line-to-line back-EMF at 1800 RPM with housing temperature....15

Figure 2.7 Calculated bearing loss from both bearings at the nominal operating temperature. 15

Figure 2.8 Measured RMS phase currents 16

Figure 2.9 Calculated copper loss at thermal equilibrium 16

Figure 2.10 Simulated (a) hysteresis and (b) eddy current losses in the GOES stator teeth, (c) coree loss in the SMC rotor poles, and (d) eddy current loss in the aluminum housing. 18

Figure 2.11 Variation of calculated bearing losses in the air gap study motor. 20

Figure 2.12 Variation of torques at different currents at 1800 RPM with different air gaps. 21

Figure 2.13 Variation of back-EMF at 1800 RPM with different air gaps. 21

Figure 2.14 Variation of copper loss with torque and total air gap at 1800 RPM. 22

Figure 2.15 Variation of other electromagnetic losses with speed and total air gap near 26.5 N*m. 22

Figure 2.16 Variation of (a) – (g) measured losses with torque and speed for different total air gaps and (h) calculated loss components at nominal operating point with total air gap. 24

Figure 2.17 Variation of (a) – (g) estimated losses with torque and speed for a normal motor with different total air gaps and (h) calculated loss components at the nominal operating point with total air gap. The estimates are produced by subtracting the calculated bearing losses from the experimental losses of the air gap study motor and replacing those bearing losses with the calculated bearing losses for the normal motor. 27

Figure 2.18 Comparison of losses for nominal motor. 29

Figure 2.19 Comparison of simulated and experimental losses for gap study motor at 1800 RPM. 30

Figure 2.20 Variation of experimental efficiency with torque and speed. 31

Figure 2.21 Pie chart of the MUT loss breakdown. 32

Figure 2.22 Variation of ZEUS motor efficiency with torque and speed [16].....33

Figure 3.1 Variation of Total Calculated Electrical Losses with Frequency 39

Figure 3.2 Variation of Torque Ripple with Switching Frequency.....43

Figure 3.3 FEA results of eddy current, hysteresis and core losses at different switching frequencies. 46

Figure 3.4 FEA results of torque ripple at different switching frequencies. 46

Figure 3.5 Electrical losses and torque ripple comparison between simulated and calculated values at different switching frequencies. 47

Figure 4.1 One stator core with copper winding in FEA model 51

Figure 4.2 FEA model of stator teeth with caps.....54

Figure 4.3 FEA simulation results in one cross section illustrate leakage flux from one stator tooth to another 55

Figure 4.4 Stator caps with adjustable thickness and height in FEA model 56

Figure 4.5 Bridge shaped stator caps with adjustable height in FEA model 57

Figure 4.6 Uneven air gap in the current motor design.....59

Figure 4.7 Flat stator OD with even air gap design 60

Figure 4.8 Sharp edge of SMC pole design 62

Figure 4.9 Variations of motor efficiency with stator cap area and average air gap. 64

Figure 4.10 Pie chart representing loss breakdown of the current and improved motor .66

Figure 4.11 FEA model showing (a) a slit on top of stator (b) physical separation splits the stator tooth.....67

Figure 4.12 Efficiency plot with different stator slit height.....68

LIST OF TABLES

Page

Table 2.1 Material used for each component in FEA model.....11

Table 2.2 Coefficients used for each component in FEA model.....29

Table 2.3 Loss breakdown of MUT at no load and 5 kW operating point.....31

Table 2.4 Loss breakdown comparison between NovaMax and ZEUS motor. 33

Table 3.1 Core Loss at Different Switching Frequencies 37

Table 3.2 Measured Harmonics Current at Different Switching Frequencies 38

Table 3.3 RMS Harmonics Current and Copper Losses 39

Table 3.4 Calculated Torque Ripple at Different Switching Frequencies 42

Table 3.5 FEA of Torque Ripple at Different Switching Frequencies.....45

Table 4.1 Impact of Stator Teeth Length on Electromagnetic Losses 50

Table 4.2 Impact of Stator Teeth Area on Electromagnetic Losses.....53

Table 4.3 Impact of stator cap size on motor efficiency at 1800 RPM.....56

Table 4.4 Efficiency comparison between separated and bridge shaped stator caps.....58

Table 4.5 Simulated loss and efficiency with flat stator OD and different cap sizes.....61

Table 4.6 Simulated loss and efficiency with sharp SMC pole 63

Table 4.7 Motor Loss Breakdown Comparison 65

Table 4.8 Motor loss breakdown comparison between NdFeb and current motor 70

1. INTRODUCTION

The US Department of Energy (DOE) Advanced Manufacturing Office's Next Generation Electric Machines: Enabling Technologies program seeks to develop ways to employ high performing materials to improve the efficiency of motors without depending on large quantities of rare earth materials [1]. The current Regal Beloit's NovaMAX® motor incorporates several innovations to achieve a state-of-the-art efficiency of 96%. As shown in Fig. 1.1, the NovaMAX motor is a dual-rotor axial flux permanent magnet (PM) motor with conically shaped air gaps. This research project is to optimize the current NovaMax motor design to further reduce the motor loss by 20%, which results in an efficiency of 96.8% at rated condition of 5 kW and 1800 RPM. Meanwhile, the design will take both manufacturability and cost into account so that the improved motor can be commercially available on the marketplace.

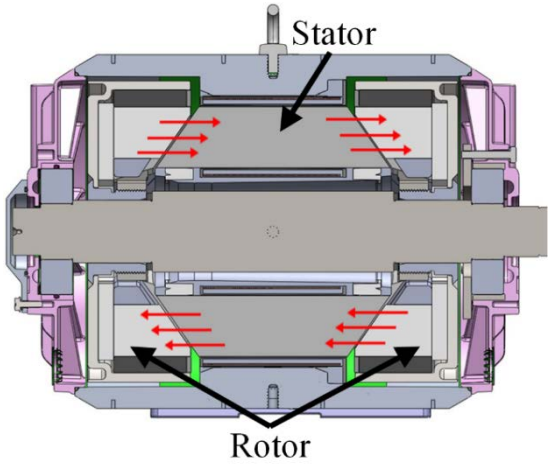

Figure 1.1 Transverse-section view of NovaMax motor with red arrows illustrating flux direction

1.1. Overview of NovaMax Motor

There are three unique topologies applied in the NovaMax motor. First is the use of grain oriented electrical steel (GOES) in stator teeth. GOES provides higher permeability, higher saturation flux density, and lower core losses than non-oriented electrical steel when flux is primarily in the direction of the grain orientation. Thus, GOES is frequently used in transformer cores; however, because most motors employ a rotating magnetic field, non-oriented steel is used in the vast majority of motors. Nonetheless, GOES has been applied to motors in a few studies [2]-[6], but the manufacturing complexity of the motor is often increased to accommodate the GOES [2]-[5]. However, as in [6], the dual rotor axial topology results in the individual stator teeth only being exposed to a pulsating axially directed flux, rather than a rotating flux, so the teeth in the NovaMAX motor are well suited for using GOES.

Second innovative design is the use of SMC material in rotor pole for flux concentration topology. As illustrated in Figure 1.2, flux from PMs in multiple directions is concentrated in soft magnetic composite (SMC) pole pieces in each rotor before crossing the air gap to the stator. The adoption of SMCs in motors has been limited because SMCs have lower permeability, lower saturation flux density, and higher hysteresis losses than steel laminations [7]-[8]. However, SMCs have a significant advantage over laminations because its properties are relatively isotropic, whereas steel laminations have lower permeability and high eddy current losses for flux normal to the laminations. Thus, SMCs have been used in motors for places where the flux paths are inherently three dimensional [8]-[10]. The flux concentration topology results in flux

travelling in all directions in the NovaMAX rotors, so the rotor pole pieces should be made of SMC, rather than laminations. Additionally, since the flux changes on the rotor are relatively small, the hysteresis losses in the SMC are relatively minor.

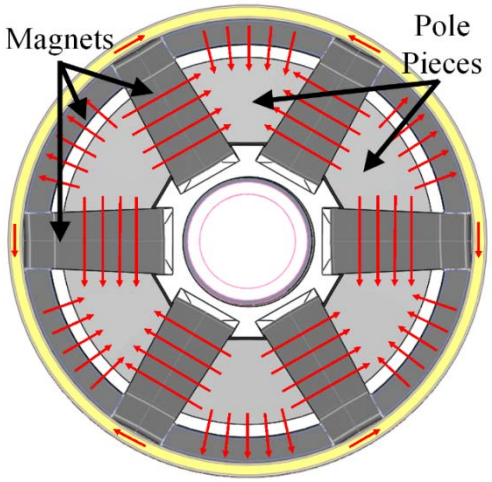

Figure 1.2 Cross-section view of one rotor of NovaMax motor with red arrows illustrating flux direction

Third innovation in NovaMax motor is the conical shaped rotor and stator which results in conical air gap. As illustrated in Figure 1.1, the air gap has a 75° angle from the shaft as oppose to 90° in conventional axial flux motors [11-13]. Conical shaped air gap creates a larger surface area relative to an axial flux motor with the same diameter, which in turn reduces the reluctance of the flux path and results in an increase in flux traveling from the rotor to stator. The flux focusing topology along with the conical air gap result in high stator flux densities, even though ferrite magnets are used instead of rare earth magnets. Since ferrite magnets have high resistivity, this also eliminates the eddy current losses that would be present in rare earth magnets. Meanwhile, use of ferrite magnet reduces manufacturing cost and make the commercial motor more

affordable. Figure 1.3 presents the view of NovaMax motor with one rotor removed, which shows conical shaped SMC pole pieces, stator GOES teeth and the use of ferrite magnets in rotor.

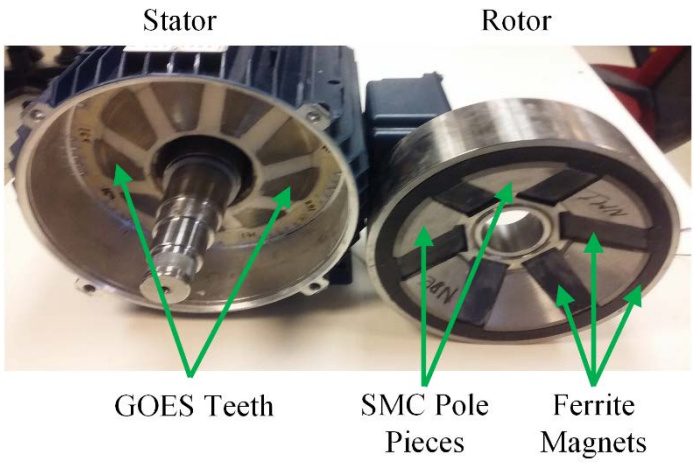

Figure 1.3 View of NovaMax motor with one rotor removed

1.2. Steps to Optimize the Motor Design

This research project consists of two phases. First phase is to create a 3D finite element analysis (FEA) model which can accurately predict the motor behavior. In this project, ANSYS Maxwell is used to produce electromagnetic related simulation results. An accurate motor geometry is obtained from computer-aided design (CAD) drawing provided by Regal Beloit, and initial material properties are obtained from manufacturer's websites. However, the material properties will need to be updated through correlating simulation results with extensive experimental results since the material properties will be altered from manufacturing process and high operating temperature. For better correlation, three different motors are tested at different operating points: a non-magnetized motor for extracting mechanical loss, a normal

motor for measuring total loss and an air gap study motor for correlating motor loss at different air gaps. The experimental test setup is shown in Figure 1.4. The motor under test (MUT) is driven by a Yaskawa A1000 variable frequency drive (VFD) operating at a switching frequency of 4 kHz. During initial testing, the switching frequency of the drive was varied between 4 kHz and 10 kHz, but this had a very minimal impact on the losses. The mechanical load is provided by a Marathon Black Max induction generator controlled by a Yaskawa U1000 VFD. The mechanical power is measured by a Himmelstein MCRT 49802V torque meter, and the electrical power input to the MUT is measured using a Yokogawa PZ4000 power analyzer.

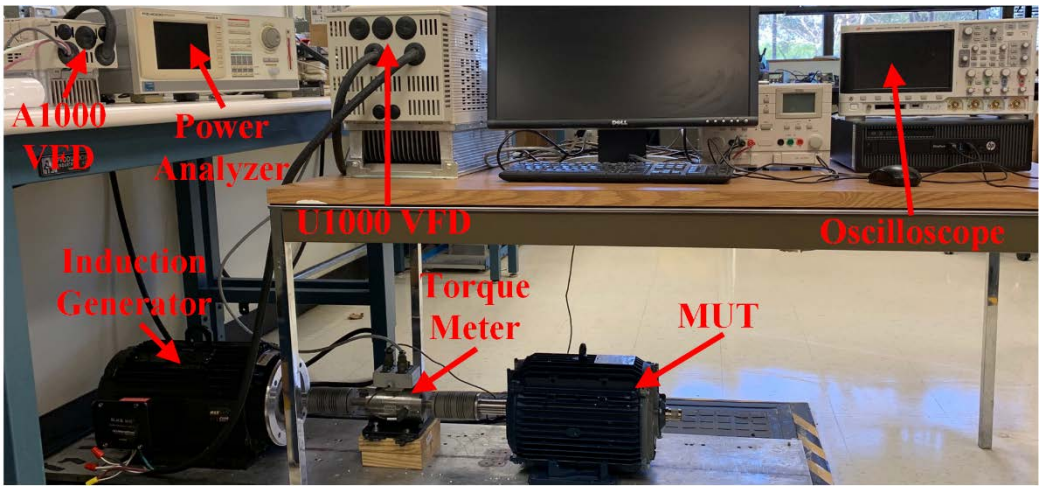

Figure 1.4 Experimental test setup with protective enclosure removed

With a wide range of experimental data collected, coefficients are used to slightly adjust the various simulated loss components to fit the experimental data more closely, using a least-squares curve fit. Additionally, the experimental data can be used for detailed motor loss breakdown. Mechanical loss can be obtained from the test results of non-magnetized motor; copper loss can be acquired from the measured resistance and

current supplied to the motor; and electromagnetic loss can be analyzed from FEA analysis results. With a detailed breakdown of current motor's losses, areas with larger portion of loss can be identified for improvements, and amount of reduction in loss can then be estimated.

Second phase of this project will be optimizing the geometry using the 3D model developed in the first phase. There are many design tradeoffs with changes in geometry. For instance, if the length of air gap reduced, flux density in the air gap will increase, and then the motor will generate more torque for the same amount of current excitation. In the other words, to generate the same level of power output, it would require less current, and thus, less copper loss. However, higher flux density will result in higher core loss in stator steel and rotor SMC piece. Details about these design tradeoffs and how they affect losses will be presented in the Section 3. To evaluate the optimal parameters that balance the loss components and give the best efficiency, extensive 3D simulations in ANSYS Maxwell are conducted.

1.3. Future Steps

After the optimal design in chosen, the next step will be producing a prototype from the parameters and geometry defined in the FEA model. Due to time constraint, this part will not be included in this thesis. However, as the next step of this research project, the advanced electric machine and power electronics (EMPE) lab at Texas A&M University will collaborate with Regal Beloit to manufacture a prototype of the updated motor designed in phase 2. Prototype motor will be ran at the rated condition of 5 kW

and 1800 RPM to verify that the proposed efficiency has been achieved, and also it will be tested at various speeds and loads to observe the motor behavior.

2. DEVELOPING AN ACCURATE 3D PARAMETRIC MODEL[1]

To analyze the motor behavior with different geometries and material properties, a parametric 3D FEA model in ANSYS Maxwell is needed as the first step. The model should be able to match the test results with sufficient accuracy to predict the final efficiency after optimizations. The goal for the first phase of this research project will be having a 3D parametric model for the current NovaMax motor that can accurately predict the losses to within 10% of the experimentally measured losses at all test points. Meanwhile, the model needs to be parametric for easy implementation of new design ideas.

2.1. Initial Model Development

ANSYS Maxwell is chosen for developing the 3D model due to its capability of modeling electromagnetic losses inside each geometry. Regal Beloit provided CAD drawing for the current NovaMax motor, so the geometry of the motor can be created in ANSYS. There are several components including shaft, motor end plates, and bearing, in which the electromagnetic losses are negligible, and therefore excluded from the model for simplification purposes. However, the mechanical loss from the bearing is significant

[1]

and will be calculated separately. An initial model developed is shown in Figure 2.1. Figure 2.1(a) illustrates flux focusing topologies with three pieces of magnet inside each pole: tangential, axial and radial magnets, which are color coded to differentiate the opposite poles. Additionally, the conical shape of SMC from Figure 2.1(a) and stator teeth from Figure 2.1(b) create a conical air gap as introduced in the previous section. Figure 2.1(c) shows the complete model based on magnetically active portions of CAD drawing provided by Regal.

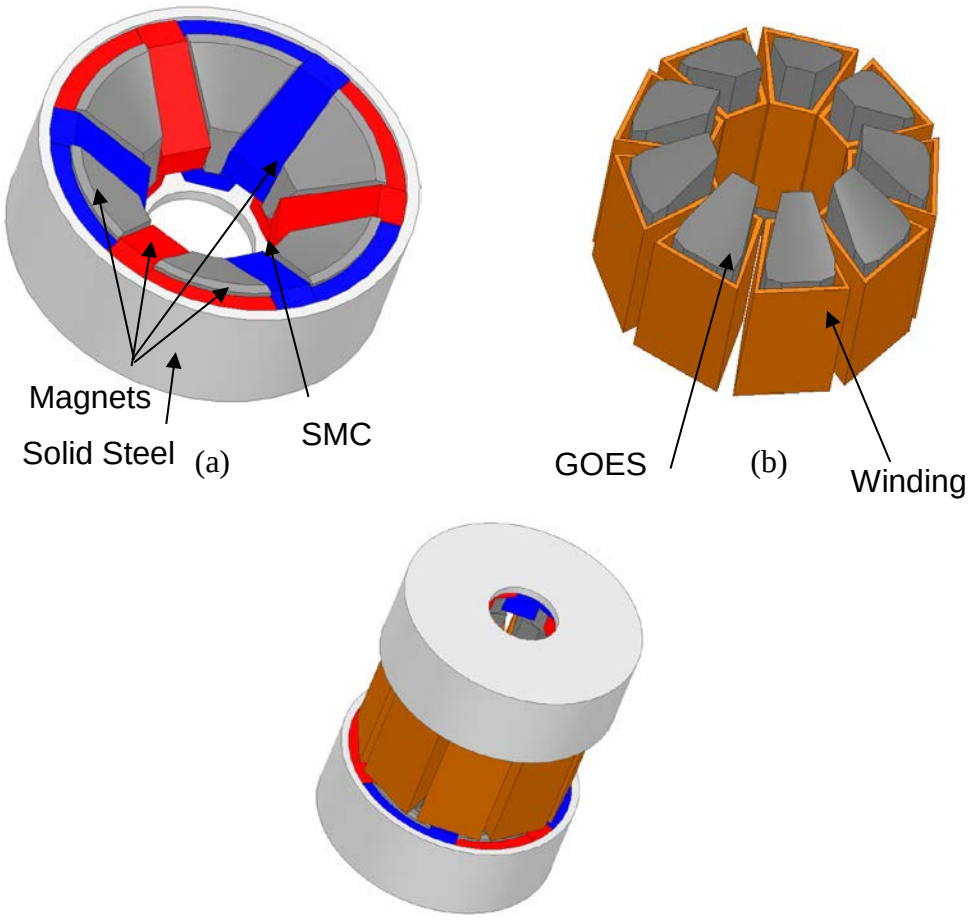

Figure 2.1 NovaMax FEA model of (a) rotor with casing, (b) stator teeth with winding, (c) full motor.

This model is fully parametric, which means any changes to the parameters will update the motor automatically. As an example, Figure 2.2 shows as parameters in FEA model change, motor geometry will be updated accordingly without the need of redesigning the model. The parametric model enables easy implementations of new design ideas.

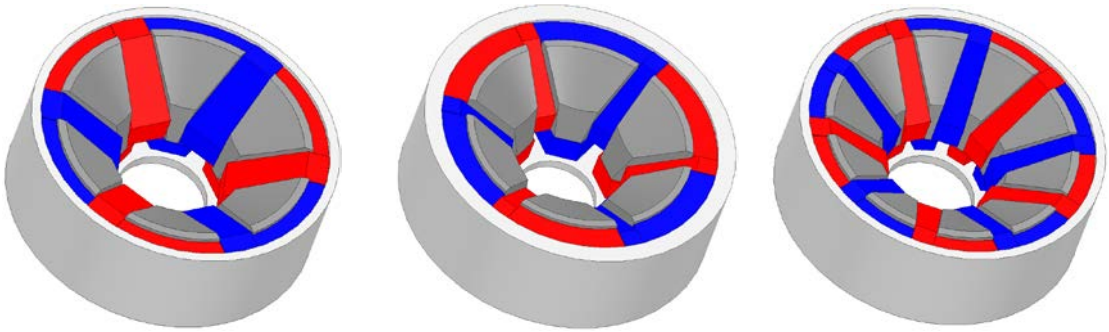

(a) (b) (c)

Figure 2.2 NovaMax FEA rotor model of (a) normal motor (b) different magnet thicknesses (c) more pole pairs.

Material used for each component can be summarized in the Table 2.1 below. Also, the material properties including permeability, conductivity, coercivity are found from manufacturer's website. Since material properties will change from machining process and operating temperature, that leads to the second step in the first phase, which is correlating the model to the actual motor.

Table 2.1 Material used for each component in FEA model

Component	Material
Stator Teeth	GOES
Rotor Pole	SMC
Rotor Magnets	Ferrite
Rotor Casing	Steel
Windings	Copper
Stator Housing	Aluminum

2.2. Motor Loss Breakdown and FEA model Correlation

Since FEA model will only analyze the electromagnetic portion of motor losses, it would be necessary to separate electromagnetic losses out from the total loss by analyzing the experimental results for an accurate correlation between the two. Meanwhile, it is a good opportunity to do a motor loss breakdown to identify the areas for improvements. The experimental setup is shown in Figure 1.4, and the test equipment is listed in Section 1.2. Main sections of losses are identified as mechanical loss, electromagnetic loss and copper loss.

2.2.1. Mechanical Losses

Friction and windage both contribute to the mechanical losses. To isolate these losses, the torque meter and mechanical load were disconnected, and no-load spindowns were performed. The mechanical loss is the derivative of the change in kinetic energy, which can be expressed as the following:

$$P_M = -\frac{dK_E}{dt} = -\frac{d}{dt}\left(\frac{1}{2}J\omega^2\right) = -J\omega(\frac{d\omega}{dt}) \quad (1)$$

where P_M is the mechanical losses, K_E is the kinetic energy, J is the moment of inertia and ω is the angular speed.

Since the inertia of the rotor is known, the loss can be calculated by measuring the speed and rate of deceleration of the motor, which was determined from the back-EMF waveforms measured using the Keysight DSO-X 3024A oscilloscope, and (2):

$$\omega = \frac{60}{2*PP*\Delta T} \quad (2)$$

where PP is the number of pole pairs and ΔT is the time between two adjacent zero-crossing voltages from the back-EMF waveform. From (2), the angular acceleration α can be calculated by taking derivative of ω as shown in (3).

$$\alpha = \frac{d\omega}{dt} \quad (3)$$

When doing no-load spindown for a normal motor, there will be core losses in addition to the mechanical loss since there will be flux created from PM, and thus it will be ideal to measure the no load spindown loss for a non-magnetized motor. However, it is hard to bring a non-magnetized motor to high speed. To solve this problem, two sets of data will be taken: one set with just the normal motor and another set with normal and non-magnetized motor's shafts mechanically connected together. After losses are calculated for both sets of data, the normal motor loss is subtracted from the loss of the data set where both motors are connected together, which determines the losses of the non-magnetized motor or the mechanical loss.

Figure 2.3 and Figure 2.4 illustrate the room temperature no-load losses of the normal motor and the non-magnetized motor. The normal motor was tested with and without both a fan and a seal. The non-magnetized motor was tested without fans or seals. Additionally, since the non-magnetized motor was not being supplied by an inverter, its shaft grounding brush could be removed. Based on these tests, the room-temperature mechanical losses from the fan, seals, and brush at 1800 RPM could be identified as approximately 9 W for the fan, 16 W for each seal, and 3 W for the shaft grounding brush. For all results presented after this point, the fan and seals have been removed from the motor to simplify the identification of losses.

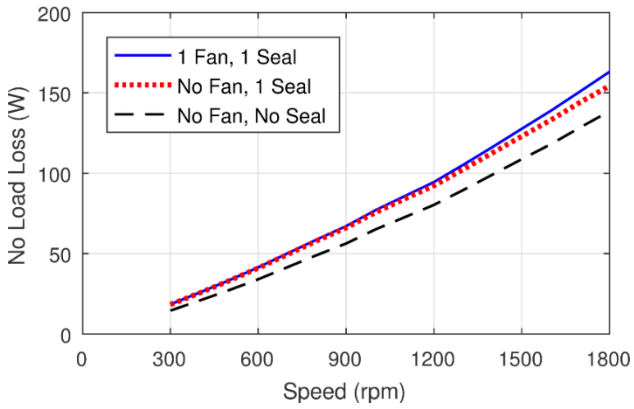

Figure 2.3 Room temperature no-load losses in the normal motor

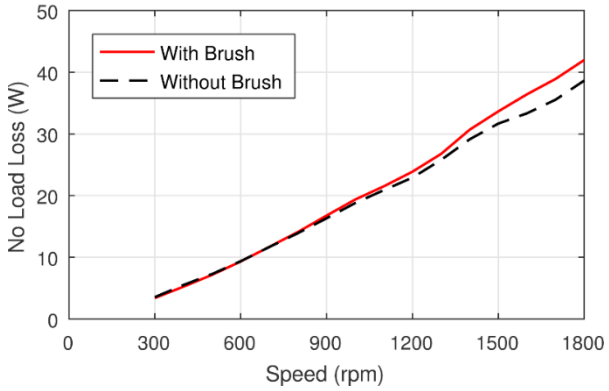

Figure 2.4 Room temperature no-load losses in the non-magnetized motor

While the previous losses were determined at room temperature, the bearing losses change significantly with temperature because the viscosity of the bearing grease is affected by bearing temperature. Figure 2.5 illustrates the no-load loss in the normal motor without fans or seals across a range of temperatures measured on the end plates near the bearings. However, the core losses also decrease as the temperature increases because the magnets produce less flux as they become warmer.

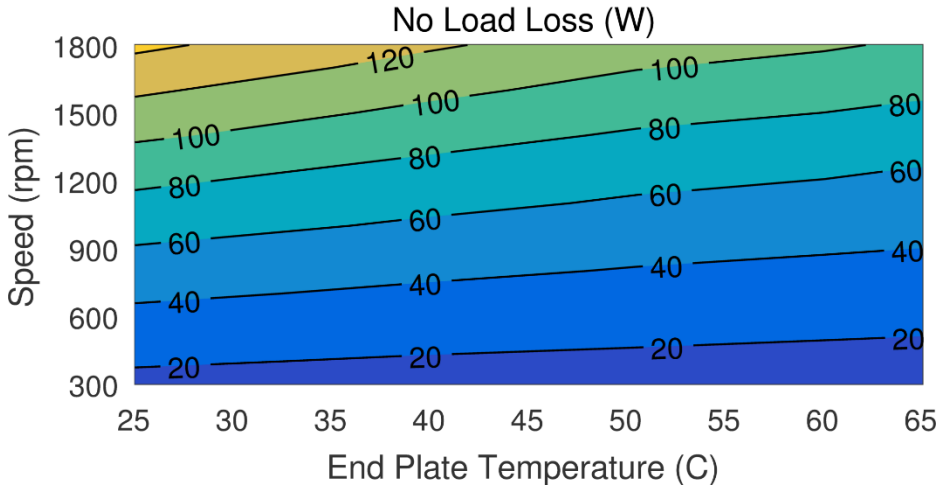

Figure 2.5 Variation of no load loss with end plate temperature and speed for the motor with no fan or seals.

Figure 2.6 illustrates the impact of the reduced flux on the back-EMF as the housing temperature increases. (Based on the results in Figure 2.4, the remanence of the PMs in the FEA was decreased by 8% from the nominal remanence at room temperature.) Therefore, the bearing losses at the nominal operating temperature are calculated using the formula provided by SKF [14] for shielded 6308 bearings. One of the inputs for this formula is the amount of force applies on the bearing, and is estimated to be 90 pounds for each bearing in this case. Figure 2.7 shows the calculated bearing

losses from both bearings versus speed after the adjustment to compensate for the uncertainties in bearing temperature and exact axial loading on each bearing.

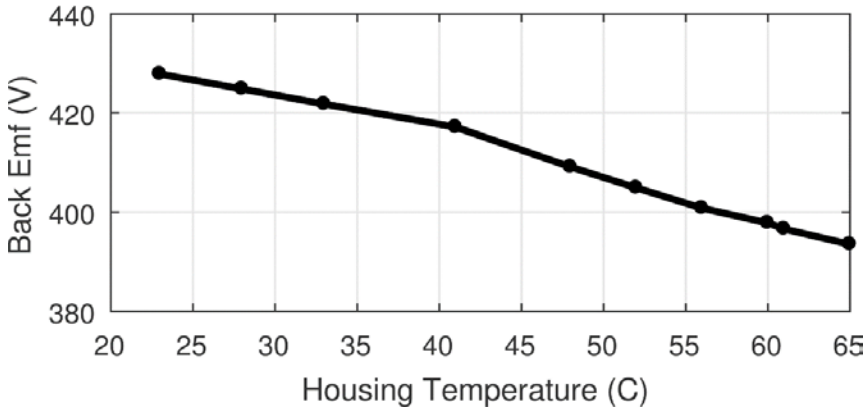

Figure 2.6 Line-to-line back-EMF at 1800 RPM with housing temperature

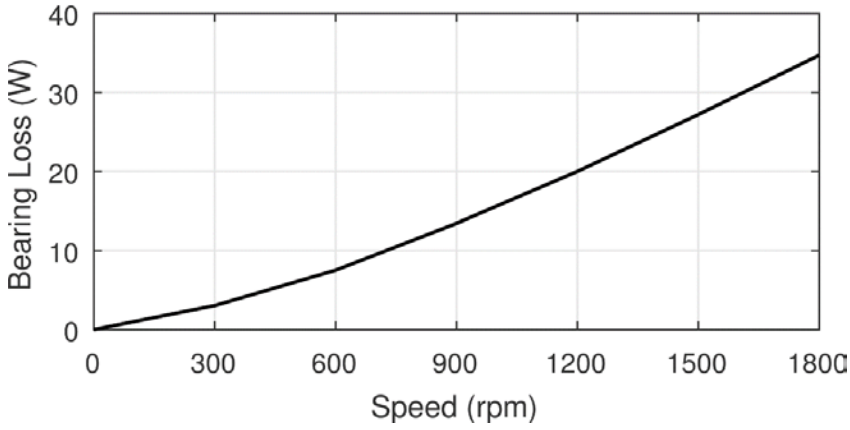

Figure 2.7 Calculated bearing loss from both bearings at the nominal operating temperature.

2.2.2. Copper Loss

Copper losses also contribute significantly to the overall losses in the MUT. For a three phase motor, assuming the line-to-line resistance R_{L-L} is the same, and the RMS phase current is measured to be I_{rms}, the copper loss can be estimated as shown in (4):

$$P_{copper} = \frac{3}{2} I_{rms}^2 R_{L-L} \quad (4)$$

Figure 2.8 shows the phase currents measured at different torques and speeds, and Figure 2.9 shows the computed copper losses according to (4).

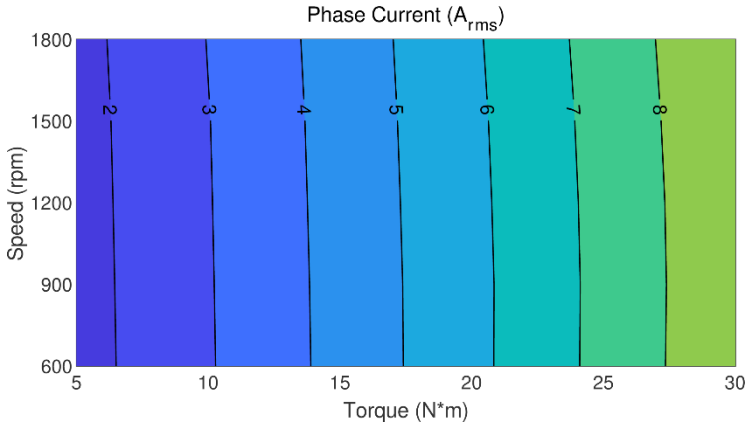

Figure 2.8 Measured RMS phase currents

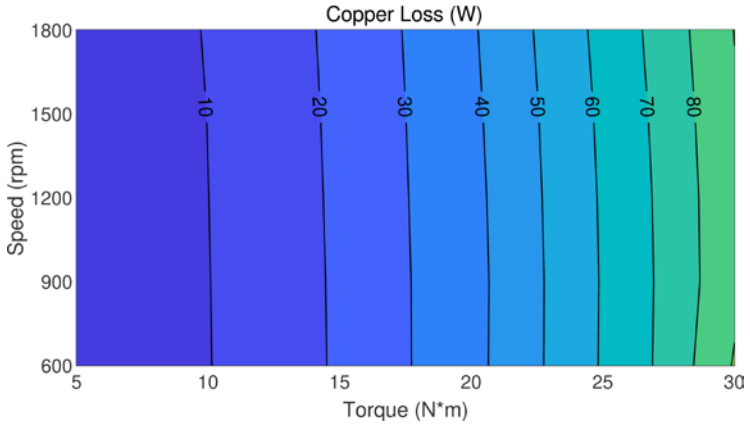

Figure 2.9 Calculated copper loss at thermal equilibrium

Theoretically, copper resistance will increase linearly with temperature according to (5):

$$R_2 = \frac{q_2 - q_0}{q_1 - q_0} * R_1 \quad (5)$$

where R_1 is the resistance at temperature q_1 and $R_2$is the resistance at temperature q_2. q_0 is the extrapolated temperature for zero resistance, which is -234.5℃ in the case of copper winding. The line-to-line resistance was measured to be 0.63 Ω at 22.5 °C. However, the MUT was run at the nominal operating point of 5 kW at 1800 RPM until the motor reached thermal equilibrium (about 60 °C on the motor housing) before taking these measurements. A thermocouple placed on the outside of the coil insulation measured temperatures very close to those measured on the surface of the case. However, the insulation results in a significant temperature difference between the copper and the thermocouple; additionally, a measurement at a single point may not accurately reflect the average temperature of the entire windings. Based on the least-squares fit, the actual line-to-line resistance at thermal equilibrium was 0.75 Ω, which would correspond to an average copper temperature of 71 °C. Figures 2.8 and 2.9 illustrate that the current and copper loss depend primarily on the torque with little impact from the speed and that the torque is very linear with current up to 30 N·m.

2.2.3. Electromagnetic Losses

The changing flux also creates significant electromagnetic losses in the MUT. The primary sources of electromagnetic losses in this motor are the core losses in the GOES stator teeth and the SMC rotor poles and eddy current losses in the aluminum housing. Since it is not practical to experimentally separate these different loss components, a commercial FEA package, ANSYS Maxwell, was used to simulate the electromagnetic loss components. Due to the uncertainty in material properties,

especially after machining, the Steinmetz coefficients for these various loss components were slightly adjusted during the least-squares fit, which will be explained in details in later section. Figure 2.10 shows the simulation results for these loss components.

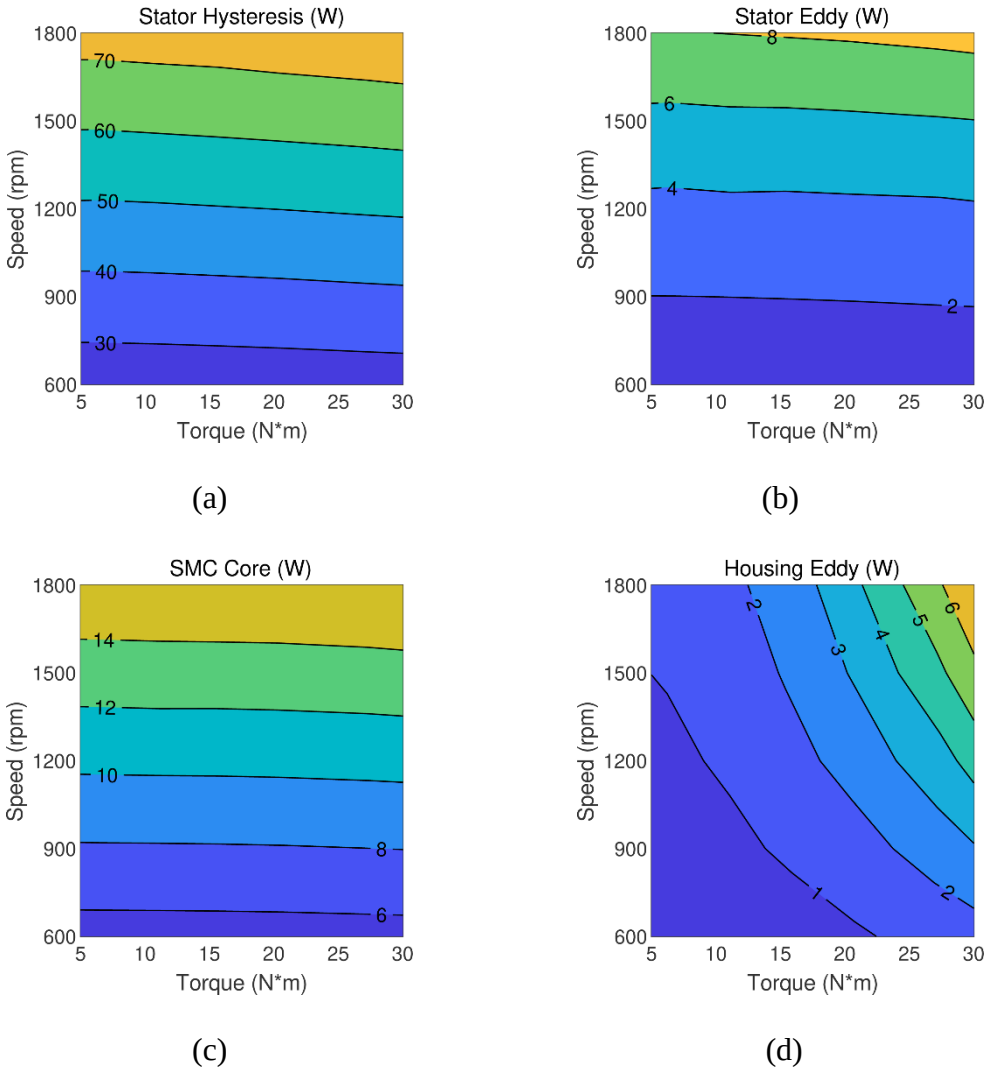

Figure 2.10 Simulated (a) hysteresis and (b) eddy current losses in the GOES stator teeth, (c) coree loss in the SMC rotor poles, and (d) eddy current loss in the aluminum housing.

Based on the simulation results, the primary source of electromagnetic losses is the core loss in the stator teeth, while the eddy current loss is much smaller than the

hysteresis loss due to the laminations. The losses in the SMC rotor poles are much smaller, so the higher hysteresis loss of SMC relative to laminated steel is not significantly harming motor performance. Additionally, there are some small eddy current losses in the aluminum housing; because these losses depend significantly on torque, they are likely caused by leakage flux from the stator winding.

2.2.4. Air Gap Study

Additionally, a prototype NovaMAX motor was constructed such that the air gaps on each side could be modified. Loss data was collected for this prototype at several different air gaps to provide further data for curve fitting the loss components and to compare with the data for the nominal motor, which has air gaps of 1.15 mm and 1.6 mm. However, the construction of the air gap study motor results in the magnetic force on each rotor being applied to their respective bearings, instead of only the net magnetic force contributing to the axial forces on the bearings. Therefore, the axial forces F_{axial} measured in previous experiments are used in the calculation of the bearing losses, which is curve fitted in (6) in terms of air gap length l_{ag}:

$$F_{axial} = 527.37 * l_{ag}^2 - 2371 * l_{ag} + 4455.5 \quad (6)$$

The estimated bearing losses is then calculated using SKF's formula, and shown in Figure 2.11 as a function of speed and air gap.

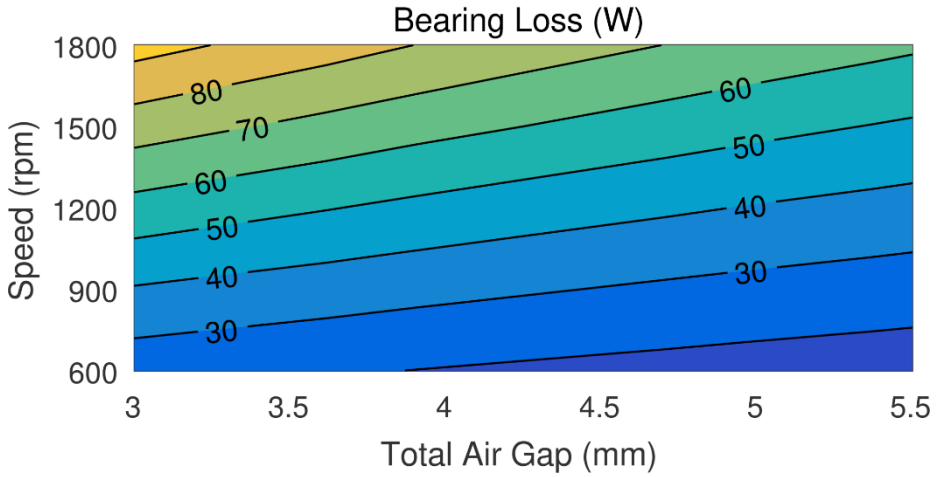

Figure 2.11 Variation of calculated bearing losses in the air gap study motor.

Additionally, the actual air gaps in the gap study motor could not be physically measured. Therefore, the air gaps were determined by comparing the measured torque per amp coefficient of the motor with simulations at different air gaps. As the air gap increases, the flux in the stator from the rotor PMs reduces according to Ampere's law presented in (7):

$$\oint H * dL = NI \tag{7}$$

where H is the magnetic field intensity, L is the length of flux path, N is the number of coil turns and I is the current in the coil. Consequently, it will reduce the torque per amp coefficient which can be explained by (8):

$$T_e = \frac{3}{2}\frac{P}{2} Im\{\lambda_{qdm}^{f*} i_{qds}^{f}\} \tag{8}$$

where T_e is the torque, λ_{qdm}^{f*} is the air gap flux in dq frame and i_{qds}^{f} is the stator current in dq frame that rotate with fundamental frequency which is 90 Hz. This is verified by experimental results shown in Figure 2.12.

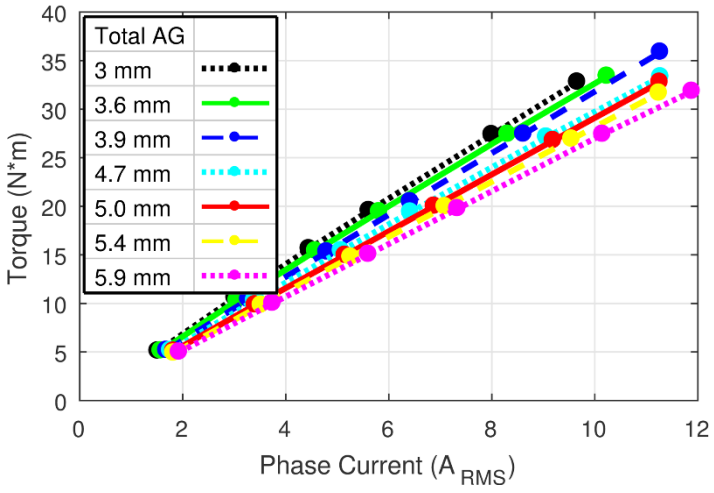

Figure 2.12 Variation of torques at different currents at 1800 RPM with different air gaps.

Thus, as the air gap increases, copper losses must increase for a given torque, whereas the other electromagnetic losses diminish due to the reduced flux linkage between the stator and the rotor. Figure 2.13 shows that increasing the air gap reduces the harmonic distortion present in the back-EMF waveform, which can further reduce core losses.

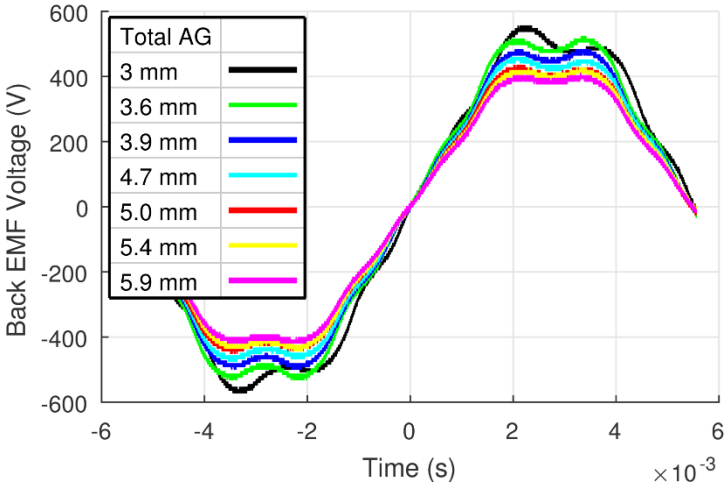

Figure 2.13 Variation of back-EMF at 1800 RPM with different air gaps.

Figure 2.14 and 2.15 show the impact of the air gap on copper losses and other electromagnetic losses.

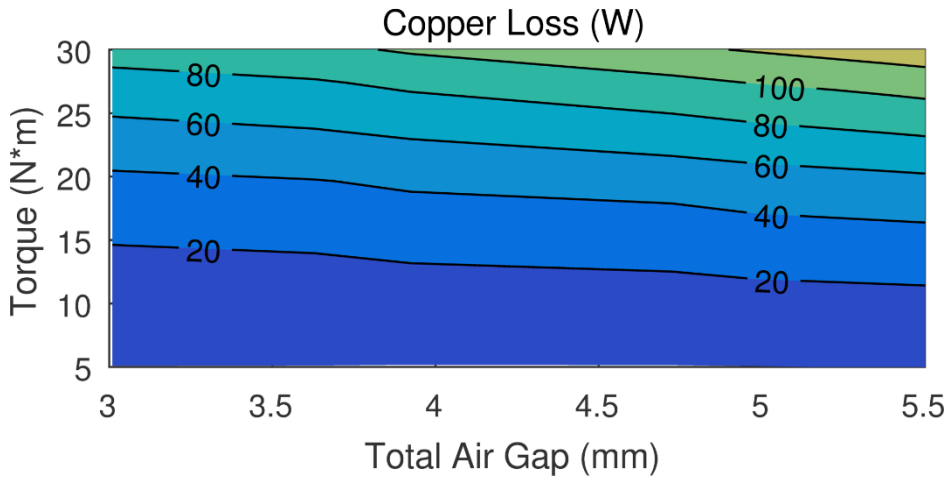

Figure 2.14 Variation of copper loss with torque and total air gap at 1800 RPM.

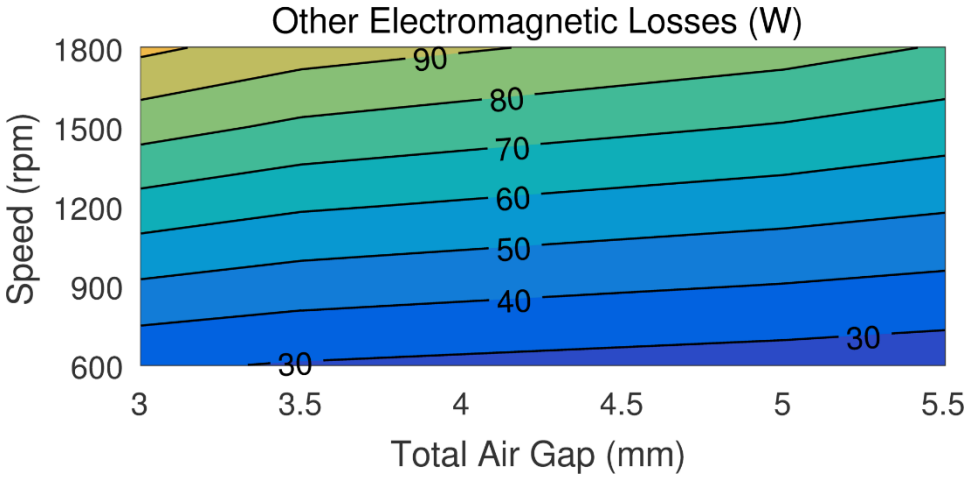

Figure 2.15 Variation of other electromagnetic losses with speed and total air gap near 26.5 N*m.

Figure 2.16 illustrates the measured losses at different air gaps. Figure 2.16 shows that, at low-speed, high-torque operation, where copper losses tend to be the dominant source of loss, the total losses are minimized with relatively small air gaps,

whereas, at high-speed, low-torque operation, where other electromagnetic losses are larger than the copper losses, losses are minimized with larger air gaps.

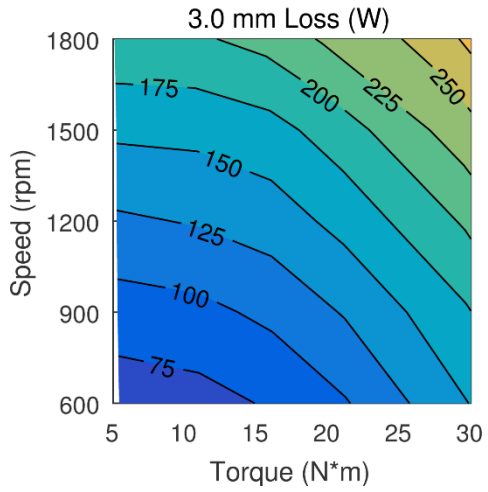

(a)

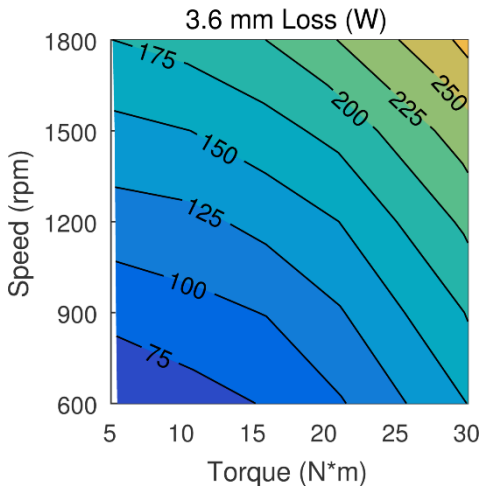

(b)

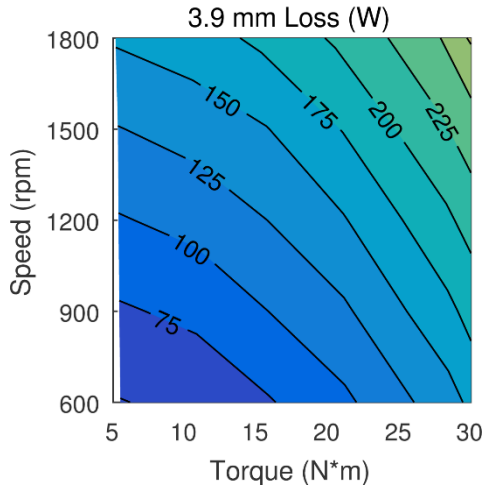

(c)

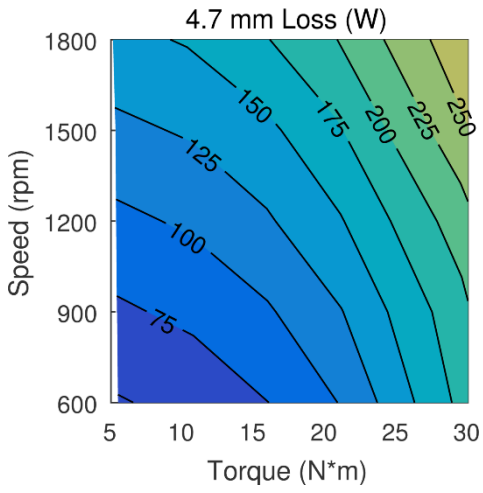

(d)

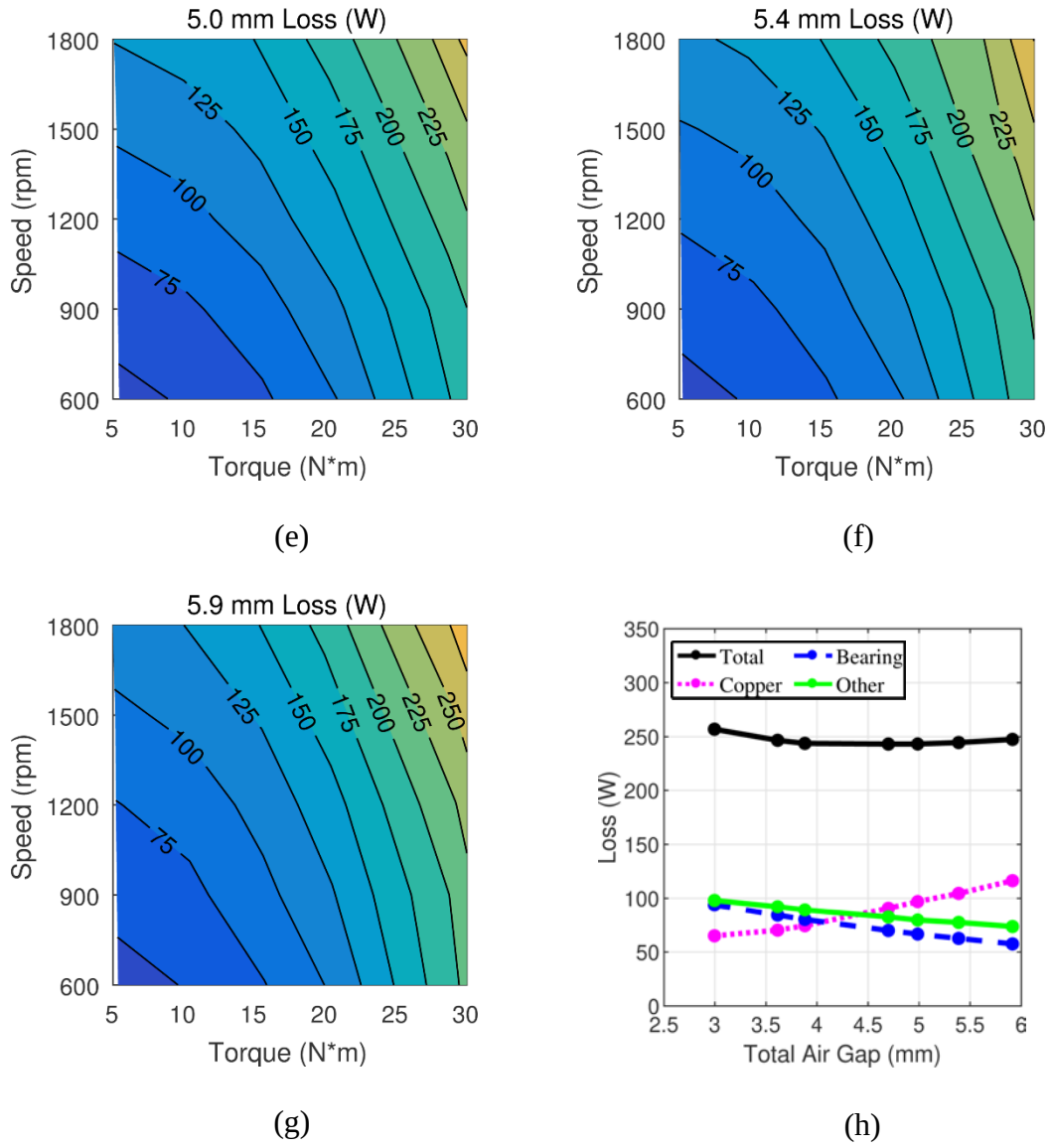

Figure 2.16 Variation of (a) – (g) measured losses with torque and speed for different total air gaps and (h) calculated loss components at nominal operating point with total air gap.

All of these cases presented in Figure 2.16 achieve lower efficiencies than the normal NovaMAX motor because the construction of the gap study motor results in larger bearing loss due to the larger axial forces on the bearings, especially at smaller total air gaps. Therefore, to provide a better representation of the losses if the motor was

built in the conventional manner with different total air gaps, Figure 2.17 shows the experimentally measured losses in the air gap study motor with the calculated bearing losses for the air gap study motor subtracted out and replaced with the calculated bearing losses for the normal motor. In this case, all the motors with different air gaps will be assumed to have the same bearing losses. This bearing loss substitution reduces the anticipated losses and the optimal air gap for the best efficiency at the nominal operating point. As the same rotor and stator geometries are used for machines with different windings, which yield different torque and speed ratings, this data indicates that significant energy savings could be achieved by using different sets of shims to provide a larger air gap for higher speed machines and a smaller air gap for lower speed machines.

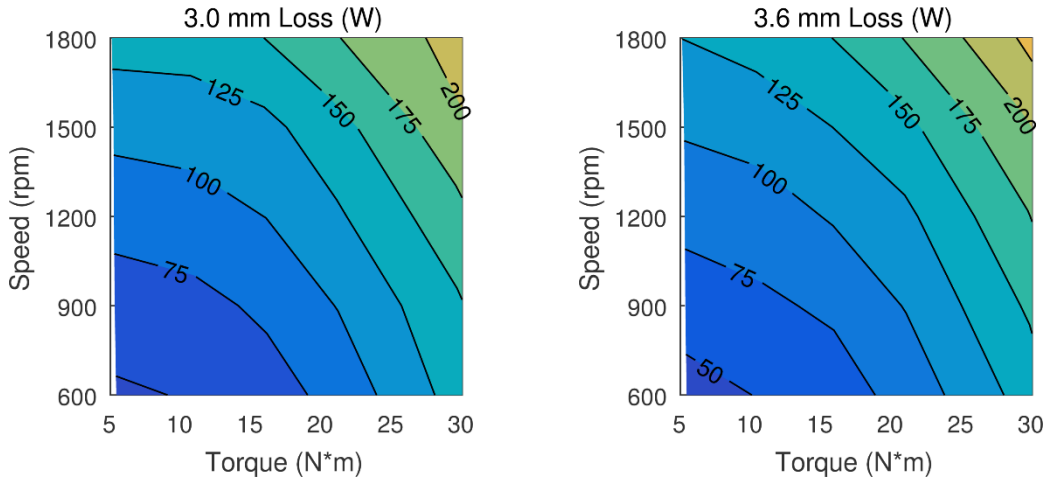

(a) (b)

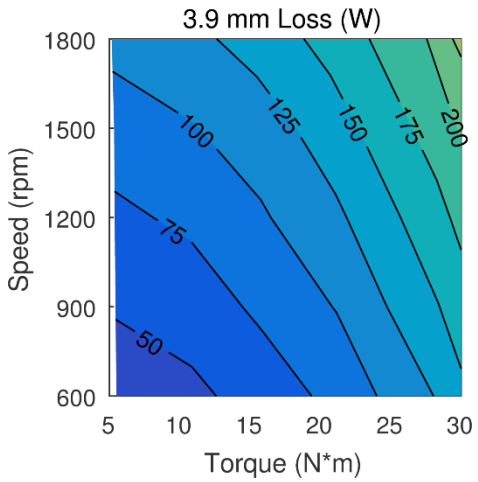
3.9 mm Loss (W)
Speed (rpm)
Torque (N*m)
1800
1500
1200
900
600
5
10
15
20
25
30
50
75
100
125
150
175
200

(c)

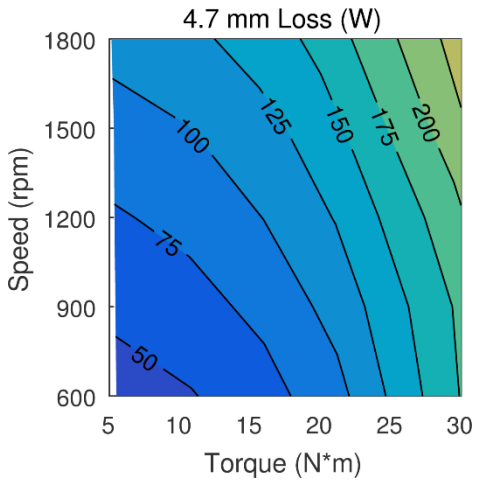
4.7 mm Loss (W)
Speed (rpm)
Torque (N*m)
1800
1500
1200
900
600
5
10
15
20
25
30
50
75
100
125
150
175
200

(d)

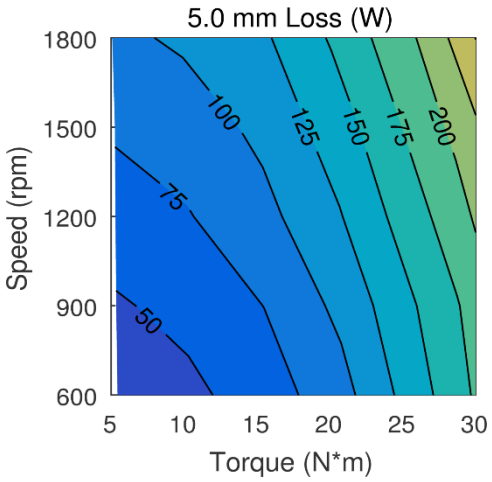
5.0 mm Loss (W)
Speed (rpm)
Torque (N*m)
1800
1500
1200
900
600
5
10
15
20
25
30
50
75
100
125
150
175
200

(e)

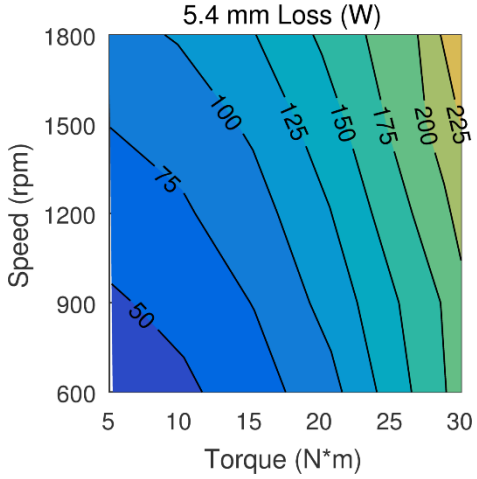
5.4 mm Loss (W)
Speed (rpm)
Torque (N*m)
1800
1500
1200
900
600
5
10
15
20
25
30
50
75
100
125
150
175
200
225

(f)

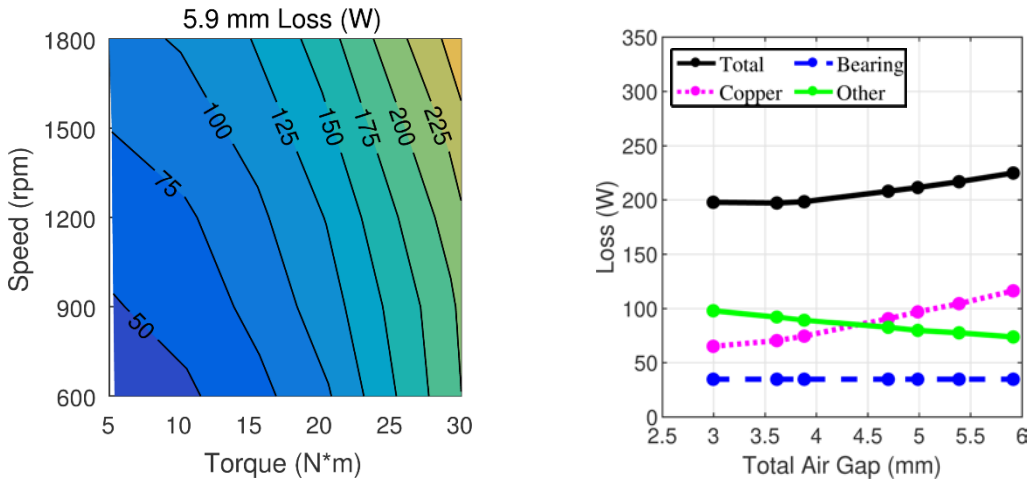

(g) (h)

Figure 2.17 Variation of (a) – (g) estimated losses with torque and speed for a normal motor with different total air gaps and (h) calculated loss components at the nominal operating point with total air gap. The estimates are produced by subtracting the calculated bearing losses from the experimental losses of the air gap study motor and replacing those bearing losses with the calculated bearing losses for the normal motor.

2.2.5. Correlating the Model to the Experimental Data

As described in the earlier sections, the material properties defined in FEA might not match the actual material properties in the experimental motor due to machining process during manufacturing and different operating temperatures. The simulation and experimental data for both normal and air gap study motors is then compared to improve FEA model's accuracy for better prediction. For fair comparison, when comparing corresponding data points from two data sets, they should have the same air gap, output torque as well as the rotor speed, and several steps are then taken for this to happen. First, since the actual air gap in the gap study motor cannot be physically measured, the torque per amp values for the gap study motor at different air gaps are calculated, and

this value is compared with the simulation torque per amp to estimate the actual air gap through interpolation. Second, torques simulated in FEA are slightly different than the experimental torques, and torques from simulations are interpolated for them to match; all the loss components are interpolated linearly with torque as well. Since MUT is a PM motor, the rotor speed ω can be controlled precisely by supplying pre-calculated frequencies f through a motor drive using (9), and thus no interpolation is needed for rotor speed.

$$f = \frac{\omega * PP}{120} \tag{9}$$

After interpolation, coefficients are applied to each loss component from simulation to have the differences between two data sets under 10%. Loss components considered here are copper loss, stator hysteresis loss, stator eddy current loss, SMC loss, stator housing loss and bearing loss. Least-squares fitting method is used to calculate the optimal coefficients so that the summed square of residuals are minimized [15]. Meanwhile, the range of coefficients in the least-squares fitting is limited to 0.8-1.2 so they will not become unrealistic for the purpose of minimizing the error. The optimal coefficients are shown in Table 2.2:

Table 2.2 Coefficients used for each component in FEA model

Component	Multiplier
Resistance	1.1076
Stator Hysteresis Loss	0.9786
Stator Eddy Current Loss	0.8
SMC Loss	1.2
Stator Housing Loss	0.8
Bearing Loss	0.8

As results from the least-squares fitting, for the nominal motor, 93% of points have error within 10%. Figure 2.18 illustrates the total losses of the MUT, and it shows a good agreement between the simulated losses after least-square fitting and the experimental losses, except at the highest torque measurements at 600 RPM. (At this point, the drive was not maintaining a constant torque, so the accuracy of the experimental data is poor. Also, it justifies limiting the range for loss coefficients so they are not calculated to compensate for the outliers.)

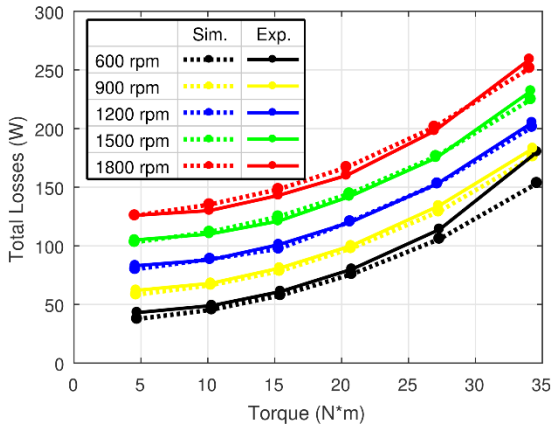

Figure 2.18 Comparison of losses for nominal motor.

For the gap study motor, 97% of data points fall within 10% of error after applying the loss coefficients, which is a good matching considering the actual air gap is estimated for the gap study motor. Figure 2.19 illustrates the losses comparison for the gap study motor at different air gaps at 1800 RPM.

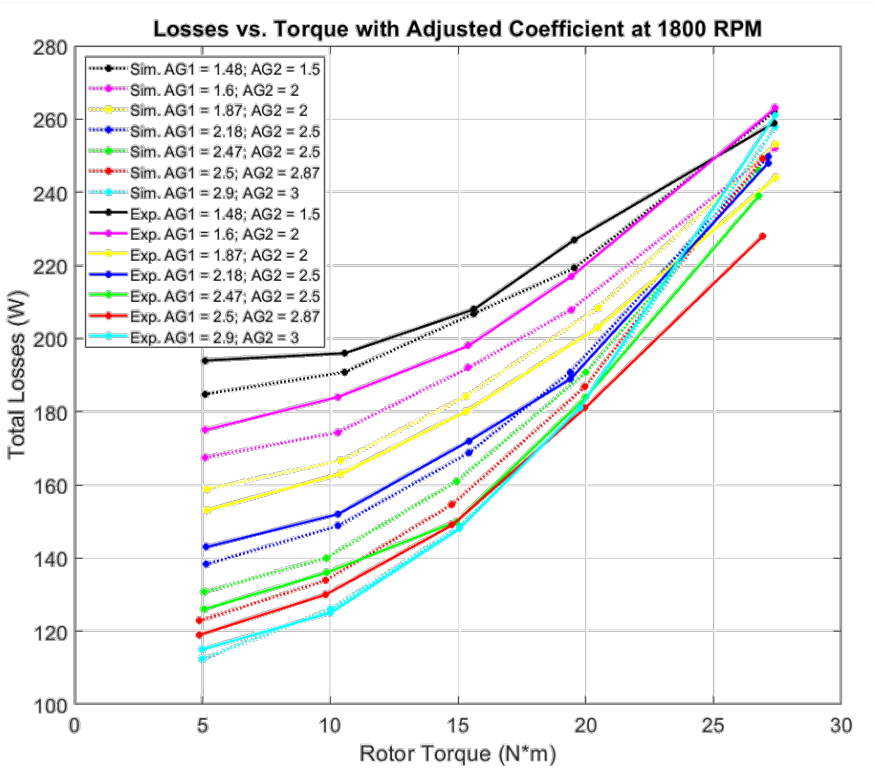

Figure 2.19 Comparison of simulated and experimental losses for gap study motor at 1800 RPM.

Fig. 2.20 illustrates that the MUT is able to achieve slightly over 96% efficiency at the nominal 1800 rpm, 5 kW operating point. Additionally, it maintains a relatively high efficiency at lower speeds. However, because the core losses and bearing losses, both of which do not vary significantly with torque, produce a large portion of the losses, the efficiency does reduce somewhat at lower torques.

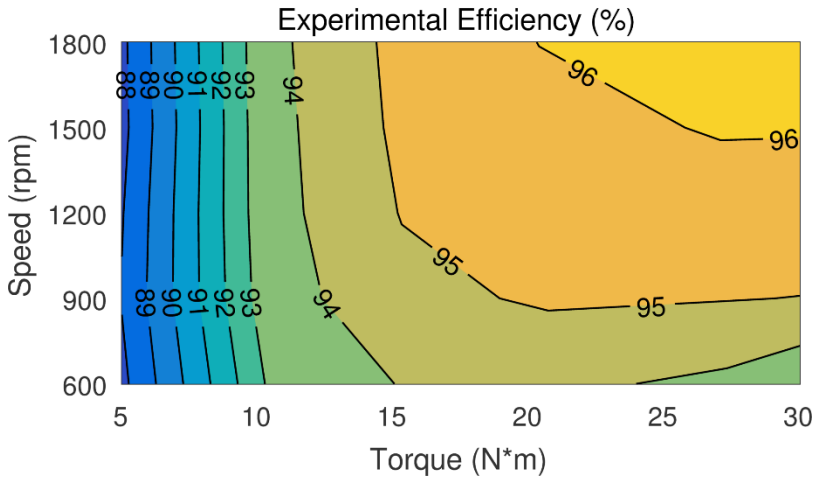

Figure 2.20 Variation of experimental efficiency with torque and speed.

Based on the loss components collected and coefficients calculated, a detailed motor loss breakdown can be analyzed as shown in Table 2.3. A visual representation is illustrated in Figure 2.21.

Table 2.3 Loss breakdown of MUT at no load and 5 kW operating point.

Loss Type	**No Load (W)**	**5 kW Operation (W)**	**Percent**
Stator Hysteresis	68.5	72.7	36%
Copper	0	64.9	32%
Bearing	34.7	34.7	17%
Rotor SMC	14.33	15.05	7%
Stator Eddy Current	6.97	7.79	4%
Stator Housing Eddy Current	0.66	6.06	3%
Total Loss	125.16	201.2	

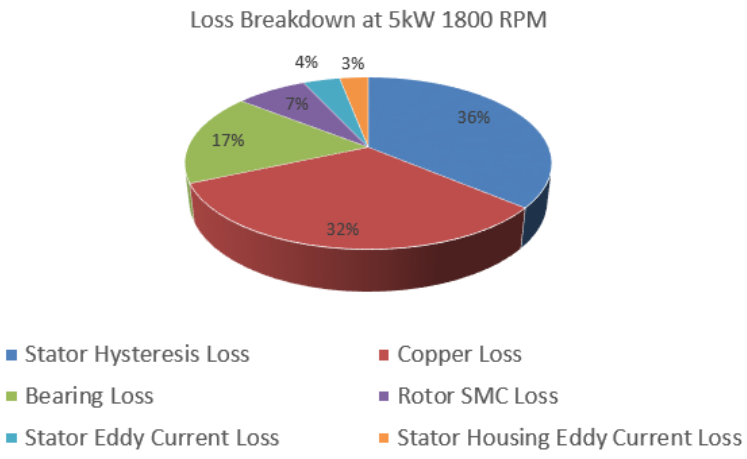

Figure 2.21 Pie chart of the MUT loss breakdown.

2.3. Loss Breakdown Comparison

To highlight the impact of some of the innovations in the NovaMAX motor and their impact on losses, the NovaMAX's losses are compared with another high-efficiency motor. The ZEUS^{TM} motor, which is rated for 11 kW at 1800 rpm, is a highly efficient radial flux motor with surface mounted rare earth PMs on the rotor [16]. Since larger motors tend to be able to achieve higher efficiencies, this does give the ZEUS motor a small advantage relative to the NovaMAX motor. Figure 2.22 shows the experimentally measured efficiency of the ZEUS motor, and Table 2.4 provides a comparison between the loss breakdowns of the NovaMAX and ZEUS motors at their nominal operating point [16]. In Table 2.4, stator core loss includes the losses in the stator teeth and the eddy current losses in the housing, and the fan and seals are not included in the friction and windage losses for the NovaMAX motor. The losses are expressed as percentages of the output power.

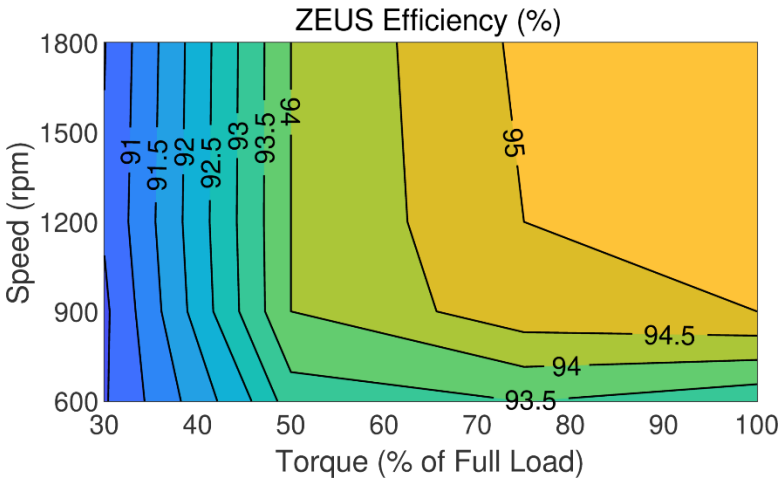

Figure 2.22 Variation of ZEUS motor efficiency with torque and speed [16].

Table 2.4 Loss breakdown comparison between NovaMax and ZEUS motor.

	NovaMax	**ZEUS**
Output Power	5000W	11470 W
Speed	1800 RPM	1800 RPM
Copper Loss	1.30%	0.85%
Stator Core Loss	1.73%	2.07%
Magnet Loss	0.00%	0.35%
Rotor Core Loss	0.30%	0.32%
Friction and Windage	0.69%	0.44%
Efficiency (%)	96.1%	96.1%

Both the NovaMAX and ZEUS motors achieve similar efficiencies, although the ZEUS motor's experimentally measured efficiency is a bit lower than predicted by the

analysis presented in Table 2.4 [16]. However, the approaches to achieving this high efficiency are different. The ZEUS motor employs rectangular wires to achieve a high copper fill factor and reduce the copper losses, whereas the NovaMAX motor employs conventional circular wires. The NovaMAX motor achieves low core losses in the stator by eliminating the stator yoke and using GOES; however, the ZEUS motor limits the peak flux densities in the stator teeth and yoke to 1.5 T and 0.9 T, respectively, whereas the NovaMAX motor has a slightly higher peak flux density of 1.6 T in the stator teeth, but the ZEUS motor still has more stator core losses than the NovaMAX motor. The NovaMAX motor has no magnet losses because its ferrite magnets have high resistivity, whereas the ZEUS motor employs axial segmentation to mitigate the losses in its rare earth magnets.

3. IMPACT OF SWITCHING FREQUENCY ON MOTOR LOSSES AND TORQUE

The experimental results in Section 2 are collected with motor drive switching frequency set to 4 kHz. However, the NovaMax's efficiency and torque performance under different drive switching frequencies need to be evaluated. For a typical motor drive, as the switching frequency increases, the inverter losses will increase due to increase in switching loss and conduction loss. To avoid overheating of the drive, the typical switching frequency ranges from 4 to 16 kHz [17]. However, the impact of the switching frequency on motor losses and torque ripple is hardly discussed in other papers.

With lower switching frequency, the amplitude of current harmonics will be larger, and vice versa. Since the motor core loss is a function of both frequency and magnetic flux density, the change in motor loss with switching frequency is not trivial. In this section, losses and torque ripple on NovaMax motor at different drive switching frequencies is investigated. Investigation will be divided into two sub-sections: theoretical analysis and FEA. Comparison and conclusion based on these results will be presented at the end of this section.

3.1. Theoretical Analysis of Impact of Switching Frequencies on Losses

Motor losses can be divided into two sections: electrical losses and mechanical losses. Mechanical losses mainly contain friction and windage losses. Although bearing friction loss will change with different flux strength, the amount of flux produced by

current harmonics is very small compare to the flux produced by permanent magnet. Thus the mechanical losses will be assumed to be the same at different switching frequencies. Electrical losses can be divided into ohmic losses and core losses. First, core loss for the motor will be discussed.

Core losses can be divided into two parts. One part of the losses is caused by change in magnetic field due to fundamental frequency while the second part is due to switching frequency. Impact of core loss from fundamental frequency will be assumed the same in this case, and thus will not be calculated. From simplified Steinmetz's equation, motor core loss can be modelled as the sum of hysteresis loss and eddy current loss by (10):

$$P_{Core} = P_h + P_e = K_h f B_m^2 + K_c (f B_m)^2 \tag{10}$$

where P_{core} is the core loss volume density due to drive switching frequency, P_h is the hysteresis loss density, P_e is the eddy current loss density, K_h is the hysteresis loss coefficient, K_c is the eddy current loss coefficient, f is the switching frequency and B_m is the magnetic flux density produced by switching harmonics. For NovaMax motor, from the B-H curve provided by manufacturer, K_h and K_c of the GOES used in stator core is approximated to be 266.2 and 0.255. At different frequencies, the value of B_m is approximated from FEA simulation, and P_{core} for different switching frequencies can be calculated by multiplying P_{core} with the stator volume which is found to be $0.001683 m^3$. The results are presented in Table 3.1.

Table 3.1 Core Loss at Different Switching Frequencies

Switching Frequency (Hz)	B_m (T)	Core Loss (W)
500	0.267	23.62
1000	0.137	16.46
4000	0.0395	13.51
6000	0.021	7.999
10000	0.014	9.289
15000	0.0089	8.181
20000	0.0066	7.868

This data shows that core loss caused by switching frequency is significant at low frequencies (<4 kHz in this case), and the numbers do not change much at high frequencies.

Copper loss due to current harmonics can be calculated by knowing the average resistance per phase and the RMS of harmonics current. RMS of harmonics current can be estimated by knowing the drive output voltages in current waveform and motor dynamic inductance matrix [18]. However, since the MUT has slotting effect, and the inductance will vary with space and time, it is hard to theoretically calculate the dynamic inductance matrix. However, an approximation can be made for the relationship between the magnitude of current ripple and switching frequency using (11) from [19]:

$$I_{pp} = \frac{V^*}{2\sqrt{3}Lf} \tag{11}$$

where V^* is the inverter output voltage, L is motor inductance and f is the switching frequency. Assuming V^* and L are the same for all switching frequencies, then the magnitude of the current ripple will be inverse proportional to the frequency. Three experimental data from previous testing is obtained, and the data is given in Table 3.2.

Table 3.2 Measured Harmonics Current at Different Switching Frequencies

Switching Frequency (Hz)	Peak Harmonics Current (A)
4000	0.338
6000	0.182
10000	0.122

Due to the limitation of the motor drive, harmonics current amplitude at other switching frequencies need to be calculated based on the experimental results from Table 3.2 and (11). Meanwhile, copper loss can be calculated since both RMS harmonics current and phase resistance are known, and the total electrical losses are approximated as the sum of copper and core losses. The estimated harmonics current, copper and total electrical losses at different switching frequencies are listed in Table 3.3.

Table 3.3 RMS Harmonics Current and Copper Losses

Switching Frequency (Hz)	RMS Harmonics Current (A)	Copper Loss (W)	Electrical Loss (W)
500	1.65	1.725	23.345
1000	0.825	0.432	16.892
4000	0.239	0.036	13.546
6000	0.129	0.011	8.01
10000	0.086	0.0047	8.294
15000	0.055	0.0019	8.183
20000	0.041	0.0011	7.869

Although copper loss is getting smaller as the switching frequency increases, it only accounts for a small portion of the electrical losses compared to the core loss. A graphical representation of the calculated electrical loss is illustrated in Figure 3.1.

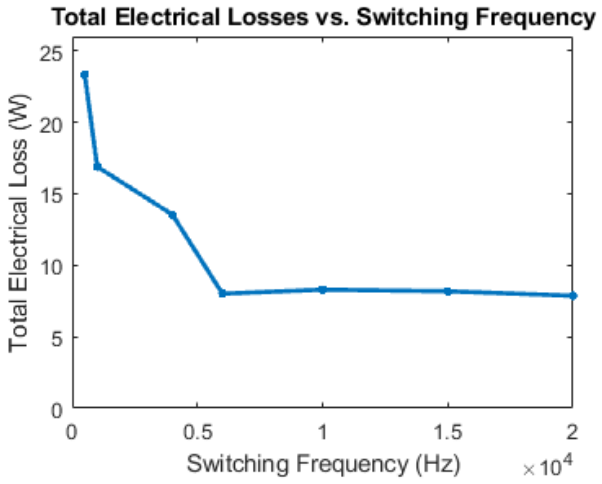

Figure 3.1 Variation of Total Calculated Electrical Losses with Frequency

From the electrical losses portion, it is observed that losses decrease substantially before 4 kHz, and the losses do not change much afterwards. Consider that low switching frequency will result in high motor loss and high switching frequency will result in high inverter loss, the optimal switching frequency for NovaMax to achieve the lowest overall loss will be around 4 kHz. However, depending on the structure and specification of each motor, the optimal switching frequency for high efficiency will be different and requires separate calculations.

3.2. Theoretical Analysis of Impact of Switching Frequencies on Torque

When transfering all the quantities from abc frame to dq frame, the motor torque can be expressed by(12) [18]:

$$T_e = \frac{3}{2}\frac{P}{2} Im\{\lambda_{qdm}^{f*} i_{qds}^{f}\} \tag{12}$$

where T_e is the torque, λ_{qdm}^{f*} is the air gap flux in dq frame and i_{qds}^{f} is the stator current in dq frame that rotate with fundamental frequency which is 90 Hz for the MUT. Now, the flux in the air gap and the stator current can be split into two parts: one part from the fundamental current and the other from the harmonics created by motor drive. Then (13) and (14) can be obtained:

$$\lambda_{qdm}^{f} = \lambda_{qdmf}^{f} + \lambda_{qdmh}^{f} \tag{13}$$

$$i_{qds}^{f} = i_{qdsf}^{f} + i_{qdsh}^{f} \tag{14}$$

where λ^{f}_{qdmf} is the flux linkage from fundamental current and λ^{f}_{qdmh} is the flux linkage of harmonics currents. Similarly, i^{f}_{qdsf} is the fundamental stator current and i^{f}_{qdsh} is the harmonics stator currents. Now, using (13) and (14), in (12) yields (15):

$$T_e = \frac{3}{2}\frac{P}{2} Im\{(\lambda^{f*}_{qdmf} + \lambda^{f*}_{qdmh})(i^{f}_{qdsf} + i^{f}_{qdsh})\}$$

$$= \frac{3}{2}\frac{P}{2} Im\{\lambda^{f*}_{qdmf}\, i^{f}_{qdsf} + \lambda^{f*}_{qdmf}\, i^{f}_{qdsh} + \lambda^{f*}_{qdmh}\, i^{f}_{qdsf} + \lambda^{f*}_{qdsh}\, i^{f}_{qdmh}\} \quad (15)$$

Since $\lambda^{f*}_{qdmf}\, i^{f}_{qdsf}$ are the fundamental components which are assumed to be the same for all switching frequencies, the first term in (15) can be ignored while calculating the torque ripple produced by the harmonics current. Then (15) can be reduced to:

$$T_h = \frac{3}{2}\frac{P}{2} Im\{\lambda^{f*}_{qdmf}\, i^{f}_{qdsh} + \lambda^{f*}_{qdmh}\, i^{f}_{qdsf} + \lambda^{f*}_{qdmh}\, i^{f}_{qdsh}\} \quad (16)$$

where T_h represents the torque produced by the harmonics currents. Since the motor investigated in this study is a PM motor, the majority of the air gap flux will be from the PM. To simplify the calculations, λ^{f*}_{qdmh} term in (16) will be ignored, and the equation can be further reduced to:

$$T_{eh} = \frac{3}{2}\frac{P}{2} Im\{\lambda^{f*}_{qdmf}\, i^{f}_{qdsh}\} = \frac{3}{2}\frac{P}{2}(\lambda^{f}_{dmf}\, i^{f}_{qsh} - \lambda^{f}_{qmf}\, i^{f}_{dsh}) \quad (17)$$

From the abc to dq transformation matrix, the following relationship (18) – (21) can be obtained:

$$\lambda^{f}_{dm} = \frac{2}{3}[\lambda_{am}\sin(\omega_f t) + \lambda_{bm}\sin\left(\omega_f t + \frac{2}{3}\pi\right) + \lambda_{cm}\sin\left(\omega_f t - \frac{2}{3}\pi\right)] \quad (18)$$

$$\lambda^{f}_{qm} = \frac{2}{3}[\lambda_{am}\cos(\omega_f t) + \lambda_{bm}\cos\left(\omega_f t - \frac{2}{3}\pi\right) + \lambda_{cm}\cos\left(\omega_f t + \frac{2}{3}\pi\right)] \quad (19)$$

$$i^{f}_{qs} = \frac{2}{3}[i_{as}\cos(\omega_f t) + i_{bs}\cos\left(\omega_f t - \frac{2}{3}\pi\right) + i_{cs}\cos\left(\omega_f t + \frac{2}{3}\pi\right)] \quad (20)$$

$$i_{ds}^{f} = \frac{2}{3}[i_{as}\sin(\omega_f t) + i_{bs}\sin\left(\omega_f t + \frac{2}{3}\pi\right) + i_{cs}\sin\left(\omega_f t - \frac{2}{3}\pi\right)] \quad (21)$$

where ω_f is the fundamental frequency and is $2\pi * 90$ in this case. From the FEA results, λ_{am} is found to be $0.6 * \sin(2\pi * 90)$ and i_{as} is the harmonics current which is listed in the Table 3.4. Phases b and c will be shifted 120° and 240°, respectively. Table 3.4 shows the calculated torque based on (17), and Figure 3.2 illustrates torque ripples at different carrier frequencies.

Table 3.4 Calculated Torque Ripple at Different Switching Frequencies

Frequency (Hz)	Peak Harmonics Current (A)	Torque Ripple (N*m)
500	2.333	6.3
1000	1.167	3.15
4000	0.338	0.913
6000	0.182	0.491
10000	0.122	0.329
15000	0.078	0.211
20000	0.058	0.157

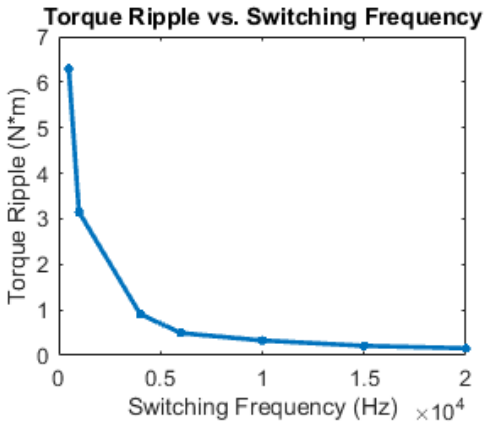

Figure 3.2 Variation of Torque Ripple with Switching Frequency

As seen in Figure 3.2, the torque ripple is large at low frequency (<4kHz) and does not change much afterwards, which aligns with the optimal frequency for good efficiency. In this case, a switching frequency around 4kHz is the frequency that can give high motor efficiency, low torque ripple while having relatively small switching losses.

One thing worth pointing out is the torque ripple caused by harmonics in experiment will be smaller than calculated. First consider the mechanical equation of motion:

$$\mathrm{J}\frac{\mathrm{d}\omega}{\mathrm{dt}} + B\omega + \mathrm{T_L} = \mathrm{T_E} \tag{22}$$

where ω is the angular speed, J is the moment of inertia of the motor, $\mathrm{T_L}$ is the load torque and $\mathrm{T_E}$ is the electromagnetic torque which is the ripple torque in this case. Take Laplace transform of (22), then (22)becomes:

$$\Omega(\mathrm{s}) = \frac{\mathrm{T_E} - T_L}{Js+B} \tag{23}$$

Equation (23) shows that the mechanical system of the motor will be a natural low pass filter which filter out the torque ripple, and thus the torque ripple caused by harmonics current in actual experiment will not be as obvious as the calculated value.

3.3. FEA of Motor Losses and Torque Ripple

For FEA, ANSYS Maxwell is used to simulate both losses and torque. Since simulating the high frequency harmonics over the whole fundamental period will be very time consuming, there are two simplifications applied to the ANSYS model. First, the harmonics injected are assumed to be sinusoidal wave. Since the drive is a three phase PWM voltage source inverter, the current harmonics will be at maximum when the duty cycle is at 50%, and 0 when duty cycle is 0 or 100%. However for the purpose of magnitude comparison, the harmonics is assumed to be a sinusoidal wave with maximum amplitude and frequency of the switching. Second assumption is that only the fundamental and one specific harmonics frequency are applied to the model. There will be more harmonics and noises produced by the drive, but only harmonics at the switching frequency will be considered in this case. Amplitude of the harmonics current used in the simulation is the calculated value from Table 3.3. The torque ripple calculated from FEA is listed in Table 3.5.

Table 3.5 FEA of Torque Ripple at Different Switching Frequencies

Frequency (Hz)	Torque Ripple (N*m)
500	6.72
1000	3.31
4000	0.938
6000	0.5
10000	0.334
15000	0.213
20000	0.162

Simulation results for hysteresis, eddy current and total core losses from harmonics are shown in Figure 3.3, and the torque ripple caused by current harmonics results are shown in Figure 3.4. The comparison between calculated and simulated results of electrical losses and torque ripple at different switching frequencies is illustrated in Figure 3.5.

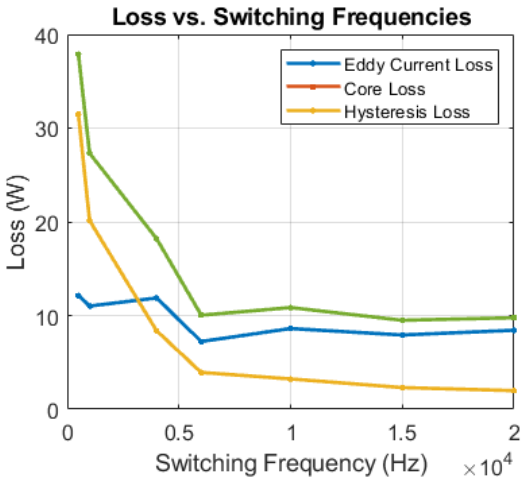

Figure 3.3 FEA results of eddy current, hysteresis and core losses at different switching frequencies.

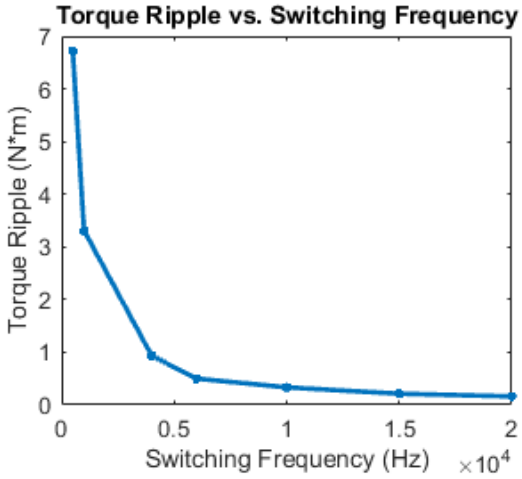

Figure 3.4 FEA results of torque ripple at different switching frequencies.

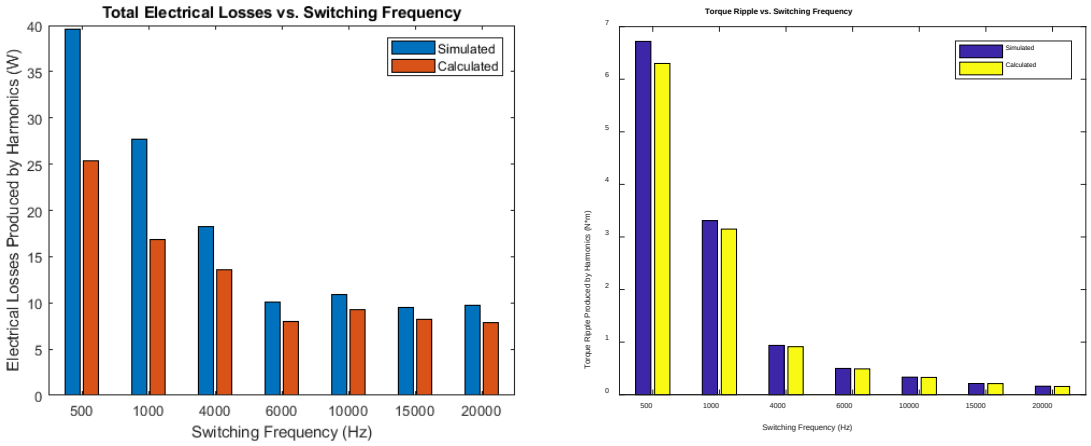

(a) (b)

Figure 3.5 Electrical losses and torque ripple comparison between simulated and calculated values at different switching frequencies.

Here, the simulated and calculated torque ripples are really close to each other. However, there are some differences for the electrical loss between the two, especially at low frequencies. One possible reason for the discrepancy is the Steinmetz equation used for calculation presented in (10). There are different versions of this equation due to skin effect of the conductors which has different exponential for B in the eddy current loss part. Nonetheless, both simulated and calculated values show the same pattern of decreasing below 4 kHz and stay around the same afterwards.

3.4. Conclusion on Impact of Switching Frequency on Motor Performance

In this section, an investigation is conducted on the impact of switching frequency on NovaMax's loss and torque through theoretical analysis and FEA. Some initial experimental data is also collected at different switching frequencies. However,

the data does not show an obvious pattern, and accuracy of the data is questionable due to inconsistency of readings from the power analyzer. Thus, the experimental data is not presented in this section to avoid confusion.

From the theoretical analysis and FEA results, for this NovaMax motor, a switching frequency around 4kHz will be ideal to get both good motor efficiency and low torque ripple while maintaining small drive losses due to high frequency switching and conduction losses. Also, motor performance is consistent for drive switching frequencies above 4 kHz.

4. DESIGN CHANGES FOR EFFICIENCY IMPROVEMENTS

As the parametric FEA model developed and calibrated for NovaMAX motor in Section 2, new design ideas need to be implemented in this section to achieve 20% reduction in motor losses, which is equivalent to 96.8% motor efficiency. Since the goal for this research project is to reduce motor losses, the output efficiency will be the figure of merit when comparing simulation results from different design changes. However, cost and manufacturability will also be considered, as this motor needs to be commercialized, with lower priority. Once motor efficiency achieves 96.8% in FEA simulation, a motor prototype will be produced by Regal incorporates the design changes in FEA. However, due to the time constraint, the production and testing of the prototype will not be covered in this thesis.

While calculating the output efficiency, both bearing loss and copper loss have been added to the electromagnetic losses from FEA. Several design ideas have been implemented and simulated, and the ones increased motor efficiency are implemented for the final design. All the attempted design changes will be presented in this section.

4.1. Reduced Volume of Stator Teeth

From the loss breakdown listed in Table 2.3, the stator core loss accounts for around 40% of the total losses, and thus it has a considerable potential for efficiency improvements. From the Steinmetz equation (10) for calculating the core loss, if the material properties stays the same, then the amount of core loss is proportional to the

volume of the material [20]. New designs for reducing the stator core volume are needed in order to reduce the stator core loss. First, reduction in the stator length is considered.

4.1.1. Stator Teeth Length Reduction

Table 4.1 lists the impact of stator teeth length on motor losses and output torque from FEA simulation results. Here, stator teeth length is changed while all other parameters kept the same.

Table 4.1 Impact of Stator Teeth Length on Electromagnetic Losses

Stator ID Length (mm)	133.54	148.54	163.5
Stator Hysteresis Loss (W)	58.6	67.14	75.5
Rotor SMC Loss (W)	13.33	13.41	13.31
Stator Eddy Current Loss (W)	8.52	9.38	10.31
Stator Housing Loss (W)	4.45	6.33	8.19

Table 4.1 verifies the prediction that amount of stator teeth length reduction corresponding to the percentage decrease in the stator core loss. Another benefit by having shorter stator teeth is that the effective stator housing is shorter; here, the effective stator housing refers to the part of the stator housing producing a noticeable amount of electromagnetic loss. The rotor casing provides a closed flux path, which shields the magnetic field inside. While the actual housing length is defined by the motor frame size, the effective stator housing length will be roughly the same as stator teeth length at outer diameter (OD), and thus the stator housing loss will be smaller by reducing the stator teeth length.

Figure 4.1 shows the current design of one stator teeth and the surrounding copper winding in FEA model. For NovaMax motor, the length of stator core is depending on the length of copper winding needed, and winding configuration needs to be reconsidered for the stator length reduction.

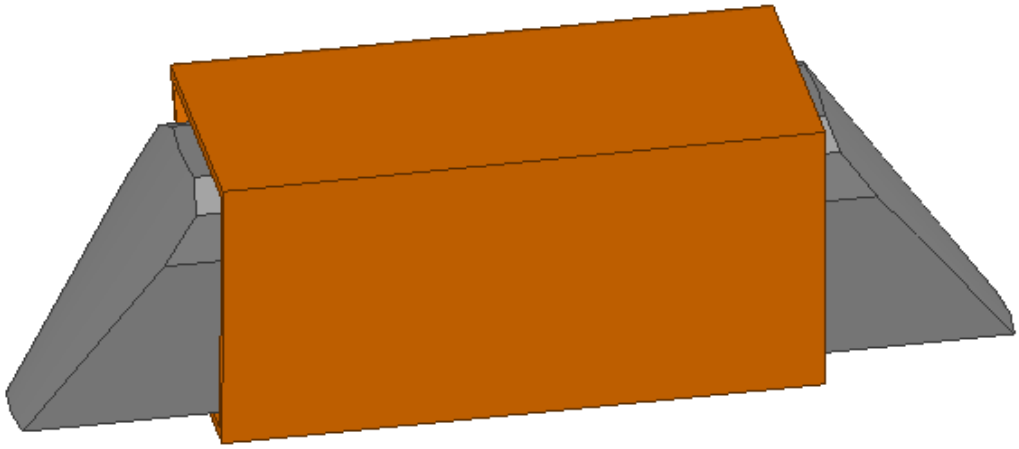

Figure 4.1 One stator core with copper winding in FEA model

There are two ways to reduce the length of copper winding, and consequently, reduce the stator core loss. First, there is a bobbin to wind the stator coil in the current motor design. However, the bobbin can be eliminated by using a technique called bobbinless winding [21], in which the windings are insulated by coating with an insulating film. By using bobbinless design, it creates more room between stator poles, and allows more layers of wires to wind on the same cross section. There are 320 turns of winding in NovaMax motor, and if the turn number is fixed, more layers of wire means the winding height can be reduced. The other way for length reduction is to use rectangular wire instead of traditional round wire. Rectangular wires have a better fill

factor [22], which not only allows more layers, but also reduce the winding height if the same turn number is used axially.

Incorporating bobbinless and rectangular wires, the updated design has 10 layers with 32 turns per layer while the current design has 4 layers with 80 turns per layer. The final stator length at interior diameter (ID) is reduced to 120 mm compared to 168.5 mm currently. The final winding configuration and stator length are decided towards the end of this phase due to evaluating the manufacturability and the cost from different suppliers, so the stator length used in FEA while evaluating some other design changes is different. However, the 120 mm stator length is implemented and simulated along with other improvements in the final design for prototyping.

4.1.2. Stator Teeth Cross Section Area Reduction

Another way of reducing the stator core volume is having smaller stator teeth cross section area. However, assuming the same flux density B, the amount of cross section area A reduced will correspond to a reduction in the air gap flux φ according to (24), and consequently reducing the torque per amp referring to (12).

$$\varphi = B * A \tag{24}$$

To produce the same output power at rated speed, 1800 RPM, more current is required, which results in more copper loss. As the core loss is reduced by having a smaller area, the copper loss is increased, and FEA simulation will be performed to evaluate the overall impact on motor efficiency.

After evaluating the motor geometry, the core area is reduced from 1354 mm^2 to 1165 mm^2, number of layers for copper winding increased from 4 to 10, and stator ID length is decreased from 168.5 mm to 128.9 mm. The FEA results for the original and updated configuration are listed in Table 4.2, where the electrical loss is the sum of electromagnetic loss and copper loss. For the one with a reduced cross section area, the input current magnitude is increased in order to have the same 5 kW output.

Table 4.2 Impact of Stator Teeth Area on Electromagnetic Losses

Stator Teeth Area (mm^2)	1354	1165
Stator ID Length (mm)	131.4	128.9
Stator Hysteresis Loss (W)	55.08	51.2
Rotor SMC Loss (W)	7.24	6.29
Stator Eddy Current Loss (W)	6.89	6.48
Stator Housing Loss (W)	2.65	5.58
Copper Loss (W)	58.12	70.34
Electrical Loss (W)	129.98	139.89

Since there is more current needed to produce the same torque for the new design, not only will the copper loss increase, but the stator housing eddy current loss will also increase as the leakage flux from stator to the housing increases. For a smaller cross section of stator teeth, although the stator core loss and SMC loss is reduced due to less flux linking stator and rotor, it cannot compensate for the increase in copper loss and

stator housing loss created by the larger current needed. Thus, the design with smaller stator teeth cross section will not be adopted in the final design.

4.2. Stator Caps

Traditional radial flux machine will have tips on the stator tooth that can increase the motor average torque and reduce the amount of cogging torque [23]-[24]. Similar to the tooth tips, the idea of adding stator caps to the current motor is proposed, and illustrated in Figure 4.2. The stator caps are made of SMC material because it is easy to shape and has low eddy current loss due to its high resistivity.

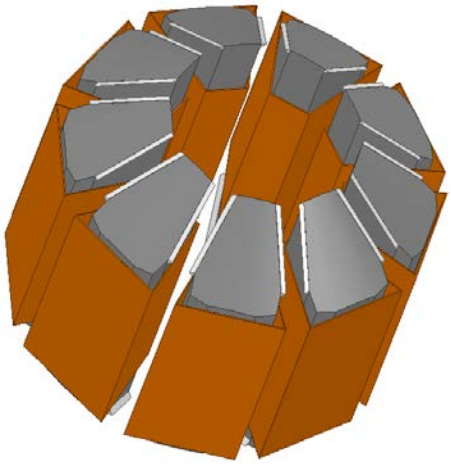

Figure 4.2 FEA model of stator teeth with caps

Since the stator caps increase the surface area, assuming flux density is the same, the amount of flux in the air gap will increase, and in turn increase the torque per amp and reduce the copper loss. Meanwhile, the caps smooth out the stator teeth surface, which reduces the cogging torque and spatial harmonics created by the slotting effect. However, the stator caps can lead to leakage flux [25] – [26] from one stator tooth to

another as illustrated in Figure 4.3, and reduce the average torque output. To find a balance between the amount of torque increased by having larger surface area and torque reduced by leakage flux, the shape of stator caps needs to be optimized.

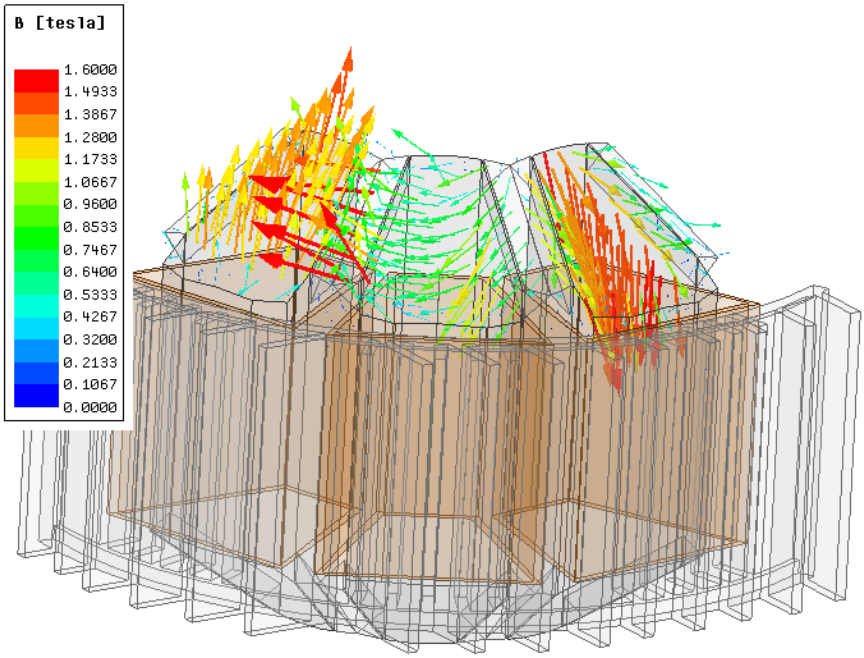

Figure 4.3 FEA simulation results in one cross section illustrate leakage flux from one stator tooth to another

4.2.1. Optimizing the Cap Shape and Size

To maximize the surface area of stator for collecting flux from rotor while minimizing the leakage flux between stator poles, the stator cap is designed to be a triangular shape as shown in Figure 4.4. The cap thickness and cap height are varied from 4mm, 4mm to 8mm, 8mm in simulations to find the design that can give the maximum motor efficiency. Results for simulations running at 1800 RPM are presented in Table 4.3.

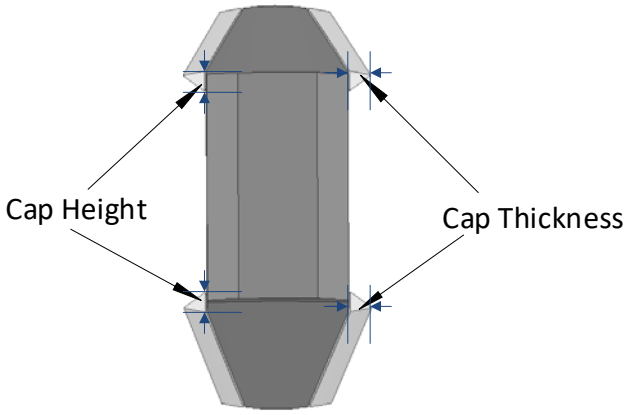

Figure 4.4 Stator caps with adjustable thickness and height in FEA model

Table 4.3 Impact of stator cap size on motor efficiency at 1800 RPM

Cap Thickness (mm)	Cap Height (mm)	Total Loss (W)	Efficiency (%)
0	0	172.32	96.67
4	4	169.8	96.71
4	6	168.96	96.76
6	6	167.79	96.76
7	7	167.21	96.69
8	2	170.19	96.69
8	4	167.51	96.79
8	6	166.78	96.8
8	8	167.06	96.77

As seen from the simulation results, the stator cap with 8mm thickness (the maximum thickness allowed without caps overlapping) has the highest efficiency, and variation of cap height between 4mm – 8mm gives roughly the same results.

Nonetheless, all the designs with stator cap achieve higher efficiency compared to the one without the stator cap.

Simulation performed in this section is an initial investigation on whether the stator cap is helping the efficiency, and the amount of improvements are expected from the stator caps. With other design changes which will be discussed in later sections, the magnetic field strength and distribution will be changed, as well as the optimal cap size. Different combinations of cap sizes will be reconsidered and simulated along with other changes for the final design.

4.2.2. Bridged Shaped Stator Caps

Stator cap designs discussed in 4.2.1 are all separate geometries without connections from one stator to another. However, another design is proposed where the stator cap is connected between stators to form a bridge shape as illustrated in Figure 4.5.

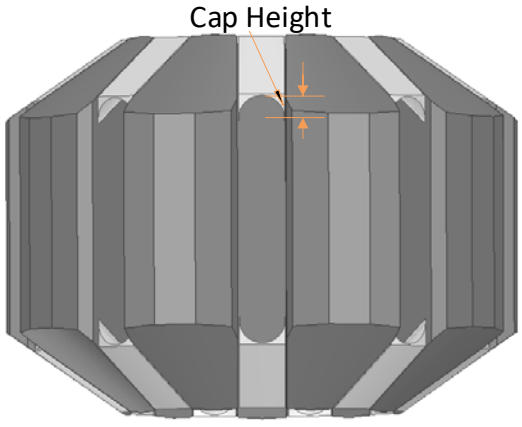

Figure 4.5 Bridge shaped stator caps with adjustable height in FEA model

In this design, the cross section area of the stator is maximized; the bridge shaped cap will try to reduce the amount of leakage flux since it is the thinnest in the middle, but there will still be more leakage flux expected compared to the previous design because the caps are physically connected. Here, the cap height is set to be 8mm and all other parameters are set to be the same as the simulations in Section 4.2.1. Simulated loss and efficiency are listed in Table 4.4.

Table 4.4 Efficiency comparison between separated and bridge shaped stator caps

	Total Loss (W)	**Efficiency (%)**
Separate Caps with 8mm, 8mm Configuration	167.06	96.77
Bridged Caps with 8mm Cap Height	173.7	96.64

From the results comparison, the bridged caps will have more loss and less efficiency compared to the separated caps configuration. This can be explained by the amount of extra flux collected by connecting the caps cannot compensate for the amount of leakage flux increased. For this reason, the separate stator caps proposed earlier will be adopted in the final design instead of the bridge shaped caps.

4.3. Increasing the Effective Air Gap Area

Current motor design includes an uneven air gap interface between stator and rotor pole as illustrated in Figure 4.6. The main reason is that the rotor pole is made of SMC which is powdered material, and cannot have sharp edges considering both mechanical strength [27] and manufacturability. However, the flat edge of SMC makes

the air gap at stator OD to be several times larger than the air gap elsewhere, and the effective air gap area is essentially smaller. As the effective area becomes smaller, it will require more current to generate same amount of torque, and thus generate more copper loss for the same reason described in previous sections. To increase the effective area, there are two design ideas proposed.

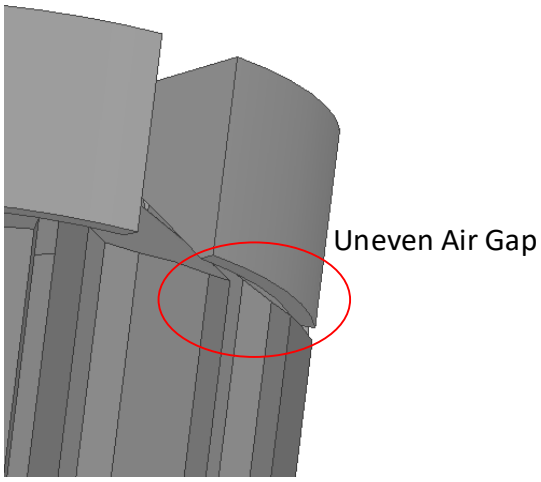

Figure 4.6 Uneven air gap in the current motor design

4.3.1. Flatten the Stator OD

One way of reducing the air gap at stator OD is to flatten the stator OD to match the shape of SMC as illustrated in Figure 4.7, which makes the air gap a combination of conical and axial shape, and there are two benefits from this design. Firstly, it enables uniform air gap throughout the whole surface of the stator pole, and thus increases the effective air gap surface area. The other benefit is that the stator core volume can be reduced by utilizing this design. The current stator OD length depends on the length of copper winding. For the new flatten OD design, the stator OD is increased while ID

remains the same, which means longer copper winding is allowed for the same ID length. In other words, if the copper winding length remains the same, the stator ID length can be reduced, and consequently the stator teeth volume can be reduced.

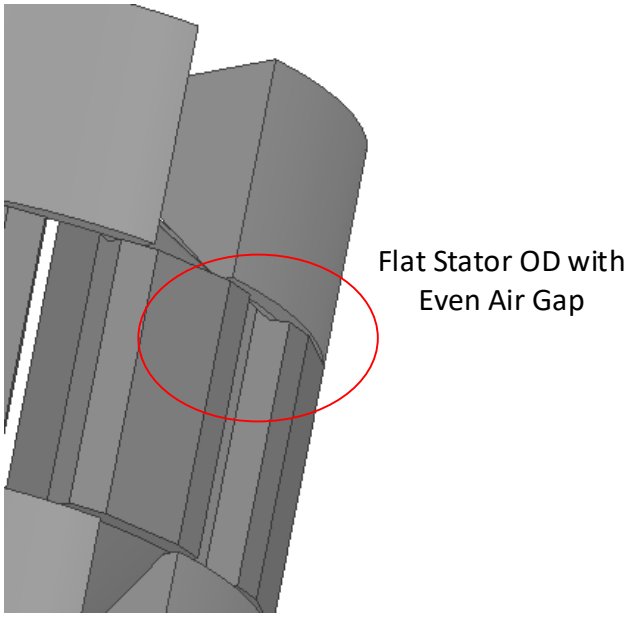

Figure 4.7 Flat stator OD with even air gap design

Considering the length reduction from the flat stator OD design, along with the rectangular wire and bobbinless winding technique, the final stator ID length is reduced to 120 mm. In this design, different stator cap sizes are also considered, and the simulation results at nominal air gap and 1800 RPM are shown in Table 4.5.

Table 4.5 Simulated loss and efficiency with flat stator OD and different cap sizes.

Cap Height (mm)	Cap Thickness (mm)	Total Loss (W)	Efficiency (%)
4	4	169.26	96.85
4	6	168.43	96.85
4	8	168.67	96.8
6	6	166.8	96.88
6	8	167	96.86
8	8	165.97	96.86

Results in Table 4.5 are all excited with standard current used in the current motor. However, the stator caps and the flat stator OD design increases the torque per amp, and thus the output power listed in this table are in the range of 5100 – 5200 W. Nonetheless, all the losses listed here are substantially lower than the 201.2 W total losses in the current motor, and efficiencies are noticeably higher than the current 96.1%. In the following section, this design will be optimized at different air gaps with appropriate magnitude of current excitation for 5 kW power output.

4.3.2. Sharper SMC Pole Edge

An alternative way of increasing the effective air gap is to make the flat part of the SMC pole smaller. Due to mechanical strength [27] and manufacturability, the SMC pole cannot be sharp. As a compromise, a new design where the SMC pole still has a flat

edge, but with a shorter flat part is proposed. To evaluate the effectiveness of this design, an extreme has been taken, where the SMC pole is made completely sharp as illustrated in Figure 4.8. Unlike the all-around good solution of the flat stator OD, the sharper SMC edge will introduce more SMC loss, and the effective air gap area increase will be less than that of flat stator OD.

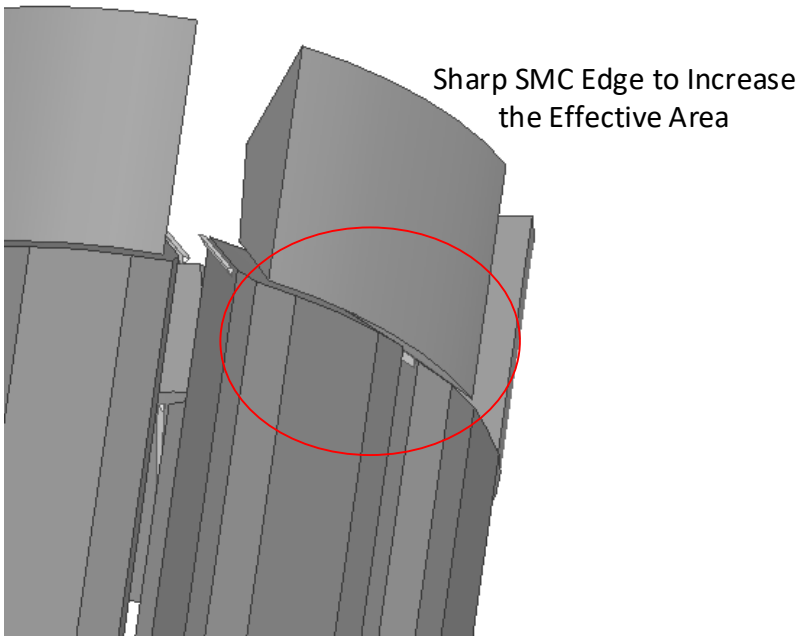

Figure 4.8 Sharp edge of SMC pole design

In this set of simulations, stator caps are also implemented to find the maximum efficiency point. The stator ID length is set to be 131mm since the rectangular wire design has not been finalized when this design is proposed, and results from these simulations will be compared against results in Section 4.2.1, where the stator length is the same and stator caps are implemented in both cases, to identify the amount of improvements. Simulation results are shown in Table 4.6.

Table 4.6 Simulated loss and efficiency with sharp SMC pole

Cap Height (mm)	Cap Thickness (mm)	Total Loss (W)	Efficiency (%)
4	4	175.16	96.71
4	6	174	96.74
4	8	173.56	96.77
6	6	172.96	96.75
6	8	172.43	96.79
8	8	171.97	96.75

When comparing these numbers with the numbers in Section 4.2.1 where only caps are implemented, the highest efficiency for both cases are 96.79%. The amount of torque increased in sharp SMC edge design might be cancelled out with increases in SMC loss and leakage flux. When only one design between the flat stator OD and sharp SMC edge has to be chosen to increase the air gap surface area, the flat stator OD is the clear winner, and thus the sharper SMC edge will not be included in the final design.

4.4. Optimal Air Gap Length Evaluation

The length of the air gap will affect motor efficiency and cannot be arbitrarily chosen. A large air gap will increase the reluctance in the flux path and reduce the amount of flux in the air gap linking rotor and stator. The amount of current needed will increase as the torque per amp constant of the motor decreases [28] – [29], and resulting the copper loss to increase. However, by having less flux collected by the stator, the

stator core loss will be reduced. Additionally, the spatial harmonics created by slotting effect will be reduced by having less flux, which reduces both rotor SMC and stator core loss.

On the other hand, a small air gap will do the opposite of what is described above. The amount of flux linking stator and rotor will increase, which increases the torque per amp and reduces the copper loss, but the stator core loss and spatial harmonics will increase at the same time.

The design with rectangular wire, bobbinless design, stator caps and flat stator OD is simulated at different air gap, and the results for overall efficiency is illustrated in Figure 4.9. For plotting purposes, the two air gap lengths are averaged, and the stator cap area is calculated assuming a right triangular cross section.

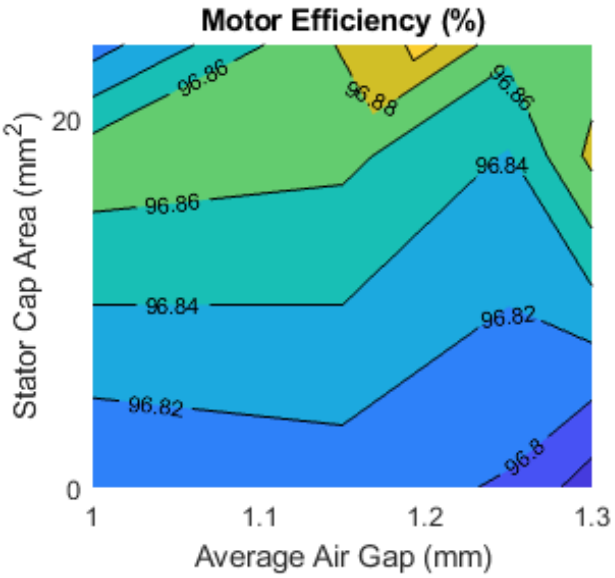

Figure 4.9 Variations of motor efficiency with stator cap area and average air gap.

Combining all the design updates, the optimal motor efficiency is simulated to be 96.91% with stator cap height of 6mm, thickness of 8 mm, and the air gap length to be 1.2 mm on both ends. Total motor loss including copper and bearing loss is estimated to be 159.1W compared to 201.2W in the current motor, which correspond to 20.9% reduction in losses. Detailed loss breakdown comparison is listed in Table 4.7, and the corresponding pie chart is illustrated in Figure 4.10.

Table 4.7 Motor Loss Breakdown Comparison

Loss Type	**Current Motor (W)**	**Percent**	**Improved Motor (W)**	**Percent**	**Reductions (W)**
Stator Hysteresis	72.7	36%	53.14	33%	19.56
Copper	64.9	32%	51.4	32%	13.5
Bearing	34.7	17%	34.7	22%	0
Rotor SMC	15.05	7%	9.99	6%	5.06
Stator Eddy Current	7.79	4%	6.31	4%	1.48
Stator Housing	6.06	3%	1.24	1%	4.82
Stator Cap	0	0%	2.86	2%	-2.86
Total Loss	201.2		159.1		42.1
Efficiency	96.10%		96.91%		

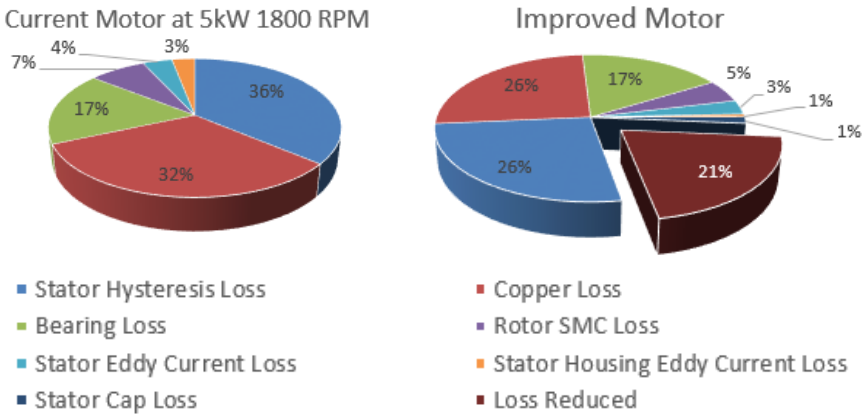

Figure 4.10 Pie chart representing loss breakdown of the current and improved motor

The goal of this project is to reduce the motor loss by 20% and achieve an efficiency of 96.8%. With updates to motor design, the FEA results show that the project goal is achieved.

4.5. Other Attempted Design Changes

There are some other design changes proposed and simulated but did not make into the final design, and they are presented in this section.

4.5.1. Slits in Stator Teeth

Referring to Figure 4.3, consider the amount of flux leaking from one stator tooth to another without producing useful torque, especially with the addition of the stator caps, the idea of having slits in stator teeth is proposed. The slits in stator teeth are

equivalent of adding air gap inside stator tooth, which creates a larger reluctance path for flux travels horizontally, and resulting in less leakage flux. There are motor slits applied in the other motors to increase the torque production [30]. However, the downside of this design is the stator tooth areas will be reduced and less flux will be collected by stator. Considering that the most flux leakage happens on top of the stator, the slits can be included on the top portion of the stator as illustrated in Figure 4.11 (a). Comparing this with the design where there is a physical separation that splits a stator tooth into two pieces as shown in Figure 4.11 (b), it reduces the reluctance of flux path in the middle of the stator.

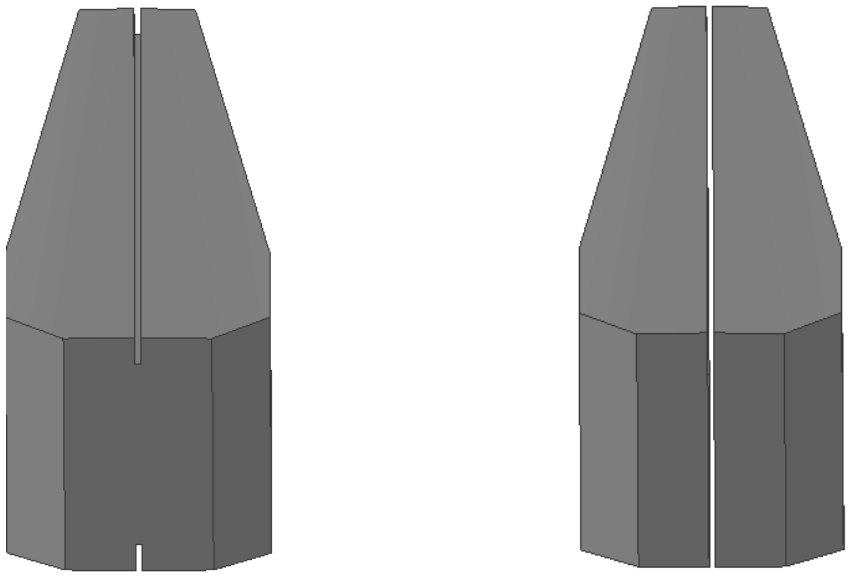

(a) (b)

Figure 4.11 FEA model showing (a) a slit on top of stator (b) physical separation splits the stator tooth.

For the geometry setup in FEA, the height of the stator slit is varied from 5mm to 20mm, and the stator caps of 8mm and 8mm is implemented for a fair comparison. The

simulation results is shown in Figure 4.12, and the one with slit height of 0mm is one does not have slit.

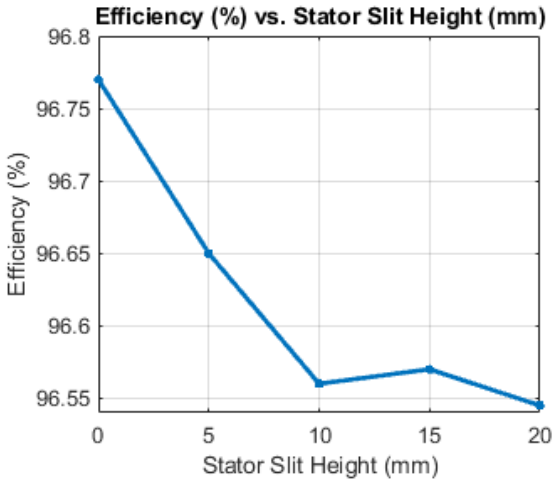

Figure 4.12 Efficiency plot with different stator slit height

From Figure 4.10, out of all configurations, the one without stator slits gives the best efficiency. It is most likely due to the amount of leakage flux eliminated cannot compensate for the reduction of flux collected by stator, therefore the slits are not included in the final design.

4.5.2. NdFeB Magnets to Replace the Existing Ferrite Magnets

In addition to the ferrite magnets, Neodymium-Iron-Boron (NdFeB) magnets are widely used in PM machines [31-33] due to its high magnetic remanence compared to ferrite magnet [31-32], which enables volume and mass reduction to achieve the same torque [33]. However, the disadvantages of NdFeB magnet are the high price [31-32], and high eddy current loss inside magnets [33].

To investigate the amount of volume and mass reduction can be achieved by using NdFeB magnets in the current motor, ferrite magnets are replaced with NdFeB for another set of FEA simulations. Although the current flux focusing topology is optimized for ferrite magnets, a direct replacement will be performed in this case to have an initial mass and volume evaluation. If the benefit is significant, then design optimization can be performed in another separate project.

Additionally, motor loss is expected to increase. For the current motor, the flux density in stator core is close to saturation; since NdFeb has much higher magnetic remanence, the amount of magnet pieces are reduced, where only the magnets magnetized in tangential direction is in the updated design to create a similar flux density. While other parameters are kept the same, there will be extra magnet loss created by NdFeb [33] compared to the ferrite magnet. Table 4.8 shows the simulation results for NdFeb magnets compared to the current design, where the ferrite density is estimated to be 5.1 g/cm^3 [34] and NdFeb density is estimated to be 7.6 g/cm^3 [35].

Table 4.8 Motor loss breakdown comparison between NdFeb and current motor

Loss Type	**Current Motor**	**Percent**	**NdFeB Motor**	**Percent**	**Reductions**
Stator Hysteresis	72.7 W	36%	79.7 W	39%	-7 W
Copper	64.9 W	32%	56.5 W	27%	8.4 W
Bearing	34.7 W	17%	34.7 W	17%	0
Rotor SMC	15.05 W	7%	16.74 W	8%	-1.69 W
Stator Eddy Current	7.79 W	4%	9.49 W	5%	-1.7 W
Stator Housing	6.06 W	3%	7.33 W	4%	-1.27 W
Magnet Loss	0	0%	2.43 W	1%	-2.43 W
Total Loss	201.2 W		206.9 W		42.1 W
Efficiency	96.10%		96.02%		-0.08%
Magnet Volume	1743 cm^3		811 cm^3		932 cm^3
Magnet Mass	8.71 kg		6.16 kg		2.55 kg

Here, the efficiency is reduced due to the geometry not being optimized for NdFeB and also the extra magnet loss introduced by it, but there are noticeable reduction in volume and mass, which agrees with the results described in other applications where NdFeB is compared to a ferrite design [36]-[37]. There are applications such as drilling for the oil and gas industry, where mass and volume of the motor is a concern and

efficiency is not the first priority, the motor designed with NdFeB can be useful. However, motor will be required to have a significant redesign if NdFeB is used instead of ferrite. Since this research project is focused on improving efficiency for a motor without relying on rare earth magnet, this proposed idea is not adopted, but it can be reevaluated in the future for other applications.

5. CONCLUSIONS AND FUTURE STEPS

5.1. Conclusions

The goal of this research project is to develop an ultra-high efficiency motor that can be cost-effectively manufactured in volume by optimizing the current NovaMax motor to achieve 20% reduction in loss. The objective is achieved at the end of the project, with a loss reduction of 20.9% as described in Section 4 of this thesis. There are three major sections contained in this thesis: developing an accurate FEA model and motor loss breakdown, investigation of the switching frequency's impact on motor torque and loss, and design improvements on FEA model.

In the first section, the losses of a NovaMAX motor have been measured and the loss breakdown is presented. Comparing the NovaMAX motor to a highly efficient radial flux surface mounted PM motor shows the impact of the innovations in the NovaMAX motor. Additionally, a study was performed where the losses were measured with different air gaps. Increasing the air gap results in larger copper losses for a given torque but lower core losses for a given speed. Based on the experimental results of nominal and air gap study motor, the FEA model is correlated and updated so the model will predict the loss within 10% of error.

Second section presented investigation of the impact of switching frequency on motor losses and torque ripple using both calculation and simulation approaches. For the NovaMax motor, switching frequency around 4 kHz will be ideal to get both good motor

efficiency and low torque ripple while maintaining small drive losses due to high switching and conduction losses.

Third section presented all the design changes applied to the current motor for final achievement of 20% reduction in motor loss, and some proposed designs which did not make to the final design are also included. Four major changes to the motor are the shorter stator core by using rectangular wires and bobbinless design, addition of separated stator caps, flattened stator teeth OD, and reevaluated air gap length. Some other design proposed including the sharp SMC pole edge, bridge shaped stator caps, slits in stator teeth, smaller stator teeth cross section and the use of NdFeB magnets.

5.2. Future Steps

As the FEA model achieves the target efficiency, a prototype motor needs to be manufactured for verification. A new round of motor loss breakdown and air gap study may be required for further FEA model adjustment.

While the design improvements performed in this research project had cost and manufacturability in mind, the efficiency is still the first priority. However, there are places where a more economical option is available with some sacrifice on efficiency such as using squeezed round wire instead of rectangular wire. These design twists might be considered in the process of having the motor commercialized.

There are some other design changes can be implemented in the future for further efficiency improvements. Some of the ideas include reevaluating the optimal angle for the conical air gap. As the conical shape gets flatter, the output torque will be lower but

the stator core volume can be reduced. There are several papers utilizing conical air gap in an axial flux motor with different cone angles [38-40], and the conical angle can be optimized for NovaMax in the future.

More aggressive design changes can be considered in the future such as the use of NdFeB magnets. A reduction in motor mass and volume with less efficiency might see a demand in some applications. However, it requires major design changes for the motor to have optimized performance for NdFeB.

REFERENCES

[1] "DE-FOA-0001467: Next Generation Electric Machines: Enabling Advanced Technologies," Office of Energy Efficiency and Renewable Energy (EERE), Mar. 9, 2016.

[2] J. Ma, J. Li, H. Fang, Z. Li, Z. Liang, L. Xiao, and R. Qu, "Optimal Design of an Axial-Flux Switched Reluctance Motor with Grain-Oriented Electrical Steel," *IEEE Trans. Ind. Appl.*, vol. 52, no. 6, pp. 5327 – 5337, Nov./Dec. 2017.

[3] Y. Sugawara and K. Akatsu, "Characteristics of a Switched Reluctance Motor using Grain-Oriented Electric Steel Sheet," in *Proc. IEEE Int. Conf. Elect. Mach. Sys.*, 2013, pp. 18 – 23.

[4] R. Pei, L. Zeng, S. Li, and T. Coombs, "Studies on grain-oriented silicon steel used in traction motors," in *Proc. IEEE Int. Conf. Elect. Mach. Sys.*, 2017, pp. 1 – 4.

[5] S. Taghavi and P. Pillay, "A Novel Grain-Oriented Lamination Rotor Core Assembly for a Synchronous Reluctance Traction Motor with a Reduced Torque Ripple Algorithm," *IEEE Trans. Ind. Appl*., vol. 52, no. 5, pp. 3729 – 3738, Sep./Oct. 2016. [6] P. M. Tlali, R.-J. Wang, and S. Gerber, "Magnetic Gear Technologies: A Review," in *Proc. Int. Conf. Elect. Mach.*, 2014, pp. 544-550.

[6] D. Kowal, P. Sergeant, L. Dupre, and A. Van den Bossche, "Comparison of Nonoriented and Grain-Oriented material in an Axial Flux Permanent-Magnet Machine," *IEEE Trans. Magn*., vol. 46, no. 2, pp. 279 – 285, Feb. 2010.

[7] G. Cvetkovski and L. Petkovska, "Performance Improvement of PM Synchronous Motor by Using Soft Magnetic Composite Material," *IEEE Trans. Magn.*, vol. 44, no. 11, pp. 3812 – 3815, Nov. 2008.

[8] A. Krings, M. Cossale, A. Tenconi, J. Soulard, A. Cavagnino, and A. Boglietti, "Magnetic Materials Used in Electrical Machines: A Comparison and Selection Guide for Early Machine Design," *IEEE Ind. Appl. Mag.*, vol. 23, no. 6, pp. 21 – 28, Nov./Dec. 2017.

[9] Y. G. Guo, J. G. Zhu, P. A. Watterson, and W. Wu, "Development of a PM Transverse Flux Motor With Soft Magnetic Composite Core," *IEEE Trans. Energy Convers.*, vol. 21, no. 2, pp. 426 – 434, June 2006.

[10] J. Asama, T. Oiwa, T. Shinshi, and A. Chiba, "Experimental Evaluation for Core Loss Reduction of a Consequent-Pole Bearingless Disk Motor Using Soft

Magnetic Composites,” *IEEE Trans. Energy Convers*., vol. 33, no. 1, pp. 324 – 332, Mar. 2018.

[11] M. Aydin, M. Gulec, Y. Demir, B. Akyuz and E. Yolacan, "Design and validation of a 24-pole coreless axial flux permanent magnet motor for a solar powered vehicle," in *2016 XXII Int. Conf. Elect. Mach. (ICEM)*, Lausanne, 2016, pp. 1493-1498.

[12] Q. D. Nguyen and S. Ueno, "Modeling and Control of Salient-Pole Permanent Magnet Axial-Gap Self-Bearing Motor," *IEEE/ASME Trans. Mechatronics*, vol. 16, no. 3, pp. 518-526, June 2011.

[13] C. Zhang, K. J. Tseng and T. D. Nguyen, "Analysis and comparison of axial flux PM synchronous motor and induction motor," *2010 Conf. Proc. IPEC*, Singapore, 2010, pp. 572-577.

[14] SKF Bearing Calculator. [Online]. Available: http://webtools3.skf.com/BearingCalc/.

[15] L. Yi and W. Y. Ping, "The realization of polynomial fit between EMF and temperature changes based on least squares fit," in *Proc. of 2011 Int. Conf. on Elect. and Mech. Eng. and Inform. Technol*., Harbin, 2011, pp. 509-512.

[16] K. W. Klontz, “Permanent Magnet Motor with Tested Efficiency Beyond Ultra-Premium/ IE5 Levels,” in *Proc. ACEEE Summer Study on Energy Efficiency in Industry*, 2017, pp. 1 – 12.

[17] Glampe, M. KEB Techonology (Tech.). [Online]. Available: https://kebblog.com/vfd-switching-frequency/

[18] Novotny, D. W., & Lipo, T. A., *Vector Control and Dynamics of AC Drives.* 1996, p. 77.

[19] G. Grandi and J. Loncarski, "Evaluation of current ripple amplitude in three-phase PWM voltage source inverters," *2013 Int. Conf. Workshop Compatibility and Power Electron.*, Ljubljana, 2013, pp. 156-161.

[20] A. J. Clerc and A. Muetze, "Measurement of stator core magnetic characteristics," in *2011 IEEE Int. Elect. Mach. and Drives Conf. (IEMDC)*, Niagara Falls, ON, 2011, pp. 1433-1438.

[21] Nittoku America. [Online]. Available: http://www.nittokuamerica.com/bobbinless-coil

[22] J. Choi et al., "Design of High Power Permanent Magnet Motor With Segment Rectangular Copper Wire and Closed Slot Opening on Electric Vehicles," *IEEE Trans. Magn.*, vol. 46, no. 6, pp. 2070-2073, June 2010.

[23] G. Li, Z. Zhu, M. P. Foster, D. A. Stone and H. Zhan, "Modular Permanent-Magnet Machines With Alternate Teeth Having Tooth Tips," *IEEE Trans. Ind. Electron.*, vol. 62, no. 10, pp. 6120-6130, Oct. 2015.

[24] I. A. A. Afinowi, Z. Q. Zhu, Y. Guan, J. C. Mipo and P. Farah, "Electromagnetic Performance of Stator Slot Permanent Magnet Machines With/Without Stator Tooth-Tips and Having Single/Double Layer Windings," *IEEE Trans. Magn.*, vol. 52, no. 6, pp. 1-10, June 2016, Art no. 8103410.

[25] T. Dong, R. Liang and L. F. Liu, "Analysis and inhibition of tooth tip leakage in the PMSM with the similar slot and pole number," in *2015 18th Int. Conf. Elect. Mach. and Syst. (ICEMS)*, Pattaya, 2015, pp. 54-57.

[26] L. Xiaohui and L. Jiahong, "An Improved Design of Slot and Tooth Dimensions of Fault-Tolerant Permanent Magnet Machine in Electromechanical Actuators," 2010 in *Int. Conf. Intell. Syst. Des. and Eng. Appl.*, Changsha, 2010, pp. 239-242.

[27] Emir Poskovic, Fausto Fanchini, Marco Actis Grande, Luca Ferraris and Robert Bidulsky, *Open Engineering*, Volume 8, Issue 1, Pages 368–372.

[28] M. Aydin and M. Gulec, "A New Coreless Axial Flux Interior Permanent Magnet Synchronous Motor With Sinusoidal Rotor Segments," *IEEE Trans. on Magn.*, vol. 52, no. 7, pp. 1-4, July 2016, Art no. 8105204.

[29] C. P. Cho, B. K. Fussell and J. Y. Hung, "Detent torque and axial force effects in a dual air-gap axial-field brushless motor," *IEEE Trans. on Magn*, vol. 29, no. 6, pp. 2416-2418, Nov. 1993.

[30] R. Hashizume, Y. Yokoi and T. Higuchi, "A Study on Iron Loss Decomposition with respect to Space Harmonics in a Slit Stator Motor," in 2018 *21st Int. Conf. Elect. Mach. and Syst.* (ICEMS), Jeju, 2018, pp. 244-247.

[31] A. D. P. Juliani, D. P. Gonzaga, J. R. B. A. Monteiro, M. L. Aguiar and A. A. Oliveira, "Magnetic Field Analysis of a Brushless DC Motor Comparing Ferrite and NdFeB Magnets on Rotor," in *2007 2nd IEEE Conf. Ind. Elect. and Appl.*, Harbin, 2007, pp. 260-264.

[32] F. Demmelmayr, B. Weiss, M. Troyer and M. Schroedl, "Comparison of PM-machines with ferrite and NdFeB magnets in terms of machine performance and sensorless start-up control," in *2013 IEEE Int. Conf. Ind. Technol. (ICIT)*, Cape Town, 2013, pp. 272-277.

[33] A. Fukuma, S. Kanazawa, D. Miyagi and N. Takahashi, "Investigation of AC loss of permanent magnet of SPM motor considering hysteresis and eddy-current losses," *IEEE Trans. on Magn*, vol. 41, no. 5, pp. 1964-1967, May 2005.

[34] TDK. Material Characteristics. [Online]. Available: https://product.tdk.com/info/en/catalog/datasheets/ferrite_mn-zn_material_characteristics_en.pdf

[35] Neo Iron Boron Magnetic Materials Properties Data. [Online]. Available: https://www.intemag.com/neo-iron-boron-magnetic-materials-properties-data

[36] M. Johnson, M. C. Gardner and H. A. Toliyat, "Design Comparison of NdFeB and Ferrite Radial Flux Surface Permanent Magnet Coaxial Magnetic Gears," *IEEE Trans. on Ind. Appl.*, vol. 54, no. 2, pp. 1254-1263, March-April 2018.

[37] F. Demmelmayr, B. Weiss, M. Troyer and M. Schroedl, "Comparison of PM-machines with ferrite and NdFeB magnets in terms of machine performance and sensorless start-up control," in *2013 IEEE Int. Conf. on Indust. Technol. (ICIT)*, Cape Town, 2013, pp. 272-277.

[38] J. Wang, C. Guo, S. Huang, X. Liu and Q. Dai, "Axial magnetic force analysis of the direct-drive radial axial flow turbine with conical-rotor PM generator," in *2017 20th Int. Conf. Elect. Mach. and Syst.(ICEMS)*, Sydney, NSW, 2017, pp. 1-4.

[39] F. Chai, K. Zhao, Z. Li and L. Gan, "Flux Weakening Performance of Permanent Magnet Synchronous Motor With a Conical Rotor," *IEEE Trans. Magn.*, vol. 53, no. 11, pp. 1-6, Nov. 2017, Art no. 8208506.

[40] P. Kascak, R. Jansen, T. Dever, A. Nagorny and K. Loparo, "Motoring performance of a conical pole-pair separated bearingless electric machine," *IEEE 2011 EnergyTech, Cleveland*, OH, 2011, pp. 1-6.